

Dissertation - II

Report on

**DESIGNING AND ANALYSIS OF DIFFERENT MODES OF TRIBOELECTRIC
NANOGENERATOR BASED SENSORS FOR IOT**

*submitted towards the partial
fulfilment of the requirements for the
award of the degree of*

Master of Science

in

Physics

Submitted by:

Vishwas Kumar

(2K21/MSCPHY/53)

*Under the supervision
of*

Prof. Vinod Singh



Department of Applied Physics

DELHI TECHNOLOGICAL UNIVERSITY

(Formerly Delhi College of Engineering)

Bawana Road, Delhi-110042

May 2023

DELHI TECHNOLOGICAL UNIVERSITY

(Formerly Delhi College of Engineering) Bawana Road, Delhi-110042

CANDIDATE'S DECLARATION

I, Vishwas Kumar (2k21/MSCPHY/53), student of M.Sc. Physics, hereby declare that the project Dissertation titled "**Designing and Analysis of Different Modes of Triboelectric Nanogenerator based Sensors for IoT**" which is submitted by me to the Department of Applied Physics, Delhi Technological University, Delhi is original and not copied from any source without proper citation. This work has not previously formed the basis for the award of any degree, diploma, associateship, fellowship or other similar title or Delhi Technological University, Delhi in partial fulfillment of the requirement for the award of the degree of Master of Science, is original and not copied from any source without proper citation. This work has not previously formed the basis for the award of any Degree, Diploma, Fellowship, or other similar title or recognition. The work has been accepted, and communicated in SCI/SCI expanded/SSCI/Scopus indexed journal or Peer-reviewed Scopus indexed conference with the following details:-

Title of Paper: Designing and Analysis of Different Modes of Triboelectric Nanogenerator based Sensors for IoT

Authors: Vishwas Kumar, Prof. Vinod Singh (Corresponding Author)

Conference Name: 4th International conference on Advances in Computing, Communication Control & Networking (ICAC3N-2022)

Status of paper (Accepted/Published/Communicated): Accepted

Name of the Journal: IEEE Xplore

Date of Paper Acceptance: August 6, 2022

Date of Conference: December 16-17, 2022

Place: Galgotias University, Greater Noida

Date: 30.05.23

VISHWAS
KUMAR

Vishwas Kumar

(2K21/MSCPHY/53)

DELHI TECHNOLOGICAL UNIVERSITY

(Formerly Delhi College of Engineering) Bawana Road, Delhi-110042

CERTIFICATE

I hereby certify that the Project Dissertation titled " **Designing and Analysis of Different Modes of Triboelectric Nanogenerator based Sensors for IoT** " which is submitted by **Vishwas Kumar (2K21/MSCPHY/53)**, Department of Applied Physics, Delhi Technological University, Delhi in partial fulfilment of the requirement for the award of the degree of Master of Science, is a record of the project work carried out by the students under my supervision. To the best of my knowledge this work has not been submitted in part or full for any Degree or Diploma to this university or any other.



Dr. Vinod Singh

(Professor)

SUPERVISOR

Place: New Delhi

Date: 30/05/2023

PUBLICATION/ACCEPTANCE RECORD



From: Microsoft CMT <email@msr-cmt.org>
Date: Sat, Aug 6, 2022, 14:09
Subject: Notification 4th IEEE ICAC3N-22 & Registration: Paper ID 1184
To: Deepak Kumar <karndeepak11@gmail.com>

Dear Deepak Kumar,
Delhi Technological University

Greetings from ICAC3N-22 ...!!!

Congratulations....!!!!!!

On behalf of the 4th ICAC3N-22 Program Committee, we are delighted to inform you that the submission of "Paper ID- 1184 " titled " Designing and Analysis of Different Modes of Triboelectric Nanogenerator based Sensors for IOT " has been accepted for presentation at the ICAC3N- 22. The conference proceedings are approved by IEEE Xplore (Conference Record Number -#56670) and Accepted papers will be submitted for inclusion into IEEE Xplore subject to meeting IEEE Xplore's scope and quality requirements.

Please complete your registration by clicking on the following Link: <https://forms.gle/8acy23i3UbtwLkFXA> on or before 15 Aug 2022.

Note:

1. All figures and equations in the paper must be clear.
2. Final camera ready copy must be strictly in IEEE format available on conference website www.icac3n.in.
3. Minimum paper length should be 5 pages.
4. If plagiarism is found at any stage in your accepted paper, the registration will be cancelled and paper will be rejected and the authors will be responsible for any consequences.
5. Violation of any of the above point may lead to rejection of your paper at any stage of publication.

CONFERENCE CERTIFICATE



4th IEEE International Conference on Advances in
Computing, Communication Control and Networking, 2022
(ICAC3N-22)

IEEE Conference Record Number #56670 & ISBN : 978-1-6654-7436-8

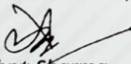
Certificate OF APPRECIATION

This is to certify that Prof./Dr./Mr./Ms. VISHWAS KUMAR of
Delhi Technological University

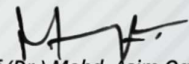
has presented a paper titled

Designing and Analysis of Different Modes of Triboelectric Nanogenerator - based Sensors for IOT


at 4th IEEE International Conference on Advances in Computing, Communication Control and Networking
(technically co-sponsored by IEEE UP Section) organised by Dept. of CSE, Galgotias College of Engineering and
Technology, Greater Noida, Uttar Pradesh, India on 16th-17th December, 2022.


Prof.(Dr.) Vishnu Sharma
Convener & Conf. Organising Chair
HoD-CSE, GCET




Prof.(Dr.) Mohd. Asim Qadri
Conf. General Chair
Director, GCET

SCOPUS INDEXING PROOF



🔍
☰

Source details

Proceedings of the IEEE

Formerly known as: Proceedings of the IRE

Scopus coverage years: from 1963 to Present

Publisher: IEEE

ISSN: 0018-9219 E-ISSN: 1558-2256

Subject area: Engineering: Electrical and Electronic Engineering Computer Science: General Computer Science

Source type: Journal

View all documents >
Set document alert
Save to source list
Source Homepage

CiteScore 2021
25.3

SJR 2021
4.678

SNIP 2021
4.366

CiteScore
CiteScore rank & trend
Scopus content coverage

i Improved CiteScore methodology ×

CiteScore 2021 counts the citations received in 2018-2021 to articles, reviews, conference papers, book chapters and data papers published in 2018-2021, and divides this by the number of publications published in 2018-2021. [Learn more >](#)

CiteScore 2021 ▼

25.3 = $\frac{11,625 \text{ Citations 2018 - 2021}}{460 \text{ Documents 2018 - 2021}}$

Calculated on 05 May, 2022

CiteScoreTracker 2022 ⓘ

31.2 = $\frac{12,851 \text{ Citations to date}}{412 \text{ Documents to date}}$

Last updated on 05 April, 2023 • Updated monthly

CiteScore rank 2021 ⓘ

Category	Rank	Percentile
Engineering		
Electrical and Electronic Engineering	#5/708	99th
Computer Science		
General Computer Science	#2/231	99th

[View CiteScore methodology >](#)
[CiteScore FAQ >](#)
[Add CiteScore to your site ↗](#)

ACKNOWLEDGEMENT

I would like to convey my heartfelt thanks to Dr. Vinod Singh, Professor, Department of Applied Physics, Delhi Technological University, for allowing me to work under his supervision and for providing me with continual inspiration and unwavering support throughout the project. I would like to take this occasion to thank my supervisor for his passionate assistance, knowledge, fantastic ideas, useful comments, and consistent support. I am appreciative of the continual assistance and convenience provided by all lab members (Ph.D. scholars), Dept. of Applied Physics, at every stage of my study. Furthermore, I am fortunate and thankful to my family and friends for their love, care, as they patiently extended all kinds of assistance to help me complete this duty.

VISHWAS
KUMAR.

Vishwas Kumar
(2K21/MSCPHY/53)

ABSTRACT

The Triboelectric Nanogenerator (TENG) has emerged as a promising technology for harvesting mechanical energy and converting it into electrical power. By leveraging the principle of triboelectrification, where electric charges are generated through frictional forces between two dissimilar materials, TENG offers a versatile and accessible approach to energy harvesting. This abstract provides an overview of TENG, including its working principle, device configurations, and potential applications. TENG is a revolutionary technology that enables the conversion of mechanical energy into electrical power through the phenomenon of triboelectrification. By exploiting the contact and separation of two dissimilar materials, TENGs generate electric charges that can be harvested as electricity. This abstract provides a concise overview of TENG, focusing on its fundamental principles, device configurations, and potential applications. TENGs offer numerous advantages, including self-powered operation, high energy conversion efficiency, and adaptability to various mechanical energy sources. They find applications in wearable electronics, IoT devices, and environmental sensors, among others, offering a sustainable and scalable approach to energy harvesting. The continued advancements in TENG technology hold great promise for addressing energy needs and powering next-generation autonomous systems and electronic devices. The voltage sensitivities of the sensor are as high as $64,000\text{Vm}^{-1}$ for contact mode and $3,00,000\text{Vm}^{-1}$ for the freestanding mode of the TENG sensor. This paper aims to design, analyse, and evaluate three modes of Triboelectric Nanogenerators (TENGs) for their potential applications in IoT, sensors, power conservation, and power generation. The designed structures possess the capability to detect minute changes in electrode separation, even at the scale of a few millimetres. A comprehensive comparison of the properties and characteristics of these TENG modes has been conducted, including the variation of open-circuit voltage and surface charge densities for a short circuit as a function of electrode separation. Additionally, the paper highlights the TENG's ability to analyse and quantify the impact of external parameters on the separation. The findings of this study provide valuable insights into the performance and potential applications of TENGs, contributing to the advancement of energy harvesting technologies and their integration into various fields.

CONTENTS

1. Title page	i
2. Candidate's Declaration	ii
3. Certificate	iii
4. Publication/Acceptance Record	iv
5. Conference Certificate	v
6. Scopus Index Proof	vi
7. Acknowledgments	vii
8. Abstract	viii
9. Contents	ix
10. List of Tables and Figures	x
11. Chapter 1: Introduction	1
12. Chapter 2: Structural Designing and Modelling	7
13. Chapter 3: Design Analysis of Software Used (COMSOL Multiphysics)	12
14. Chapter 4: Results and Simulation	21
15. Chapter 5: Conclusion and Future Scope	34
16. References	38
17. Plagiarism Report	40
18. Published Paper	41

LIST OF TABLES

Table 3.1 Variables

Table 3.2 Variables

Table 4.1 Sensitivities of different modes of TENG based sensors

LIST OF FIGURES

Fig 1.1 Device structure

Fig 2.1 Structure and working illustration of the Triboelectric generator with the stacking of positive and negative layers. (a) Circuit diagram showing TENG in contact separation mode with a contact separation of d millimetres. (b) Circuit diagram of TENG in contact sliding mode with the positive and negative charges separated and connected with voltage source V . (c) Circuit diagram of TENG in free-standing mode with the positive and negative charges separated and connected with voltage source V .

Fig 2.2 The designed geometry for the TENG modes with stacked layers with the top and bottom layers being Al_2O_3 electrodes and in the middle being the thin nanofilm of polyethylene. (a) Layers of electrodes for contact mode with contact separation being of the order of a few millimetres (b) The designed structure for the sliding layers of the sliding mode TENG. (c) Freestanding mode designed structure for TENG with two electrodes below and single electrode above them and the polyethylene film between the electrodes.

Fig 3.1 Materials

Fig 3.2 Materials Parameters

Fig 3.3 Charge Conservation

Fig 3.4 Mesh Model

Fig 3.5 Solution Model

Fig 3.6 Surface: Surface charge density (pC/m^2) Streamline: Electric field Streamline Color: Electric field norm (V/m)

Fig 4.1. The mesh structure for the TENG geometry showing the minute details of the electrodes and their separation.

Fig 4.2 Electric field norm of contact mode TENG showing the distribution of the electric field when the electrodes that are positive and negative are close to each other. With the Polyethylene layer being negative and the Al_2O_3 layers being positive. The distance of separation for (a) $d=0.006\text{m}$ (b) $d=0.013\text{m}$ (c) $d=0.016\text{m}$ and (d) $d=0.019\text{m}$.

Fig 4.3 Open circuit voltage versus contact separation distance curve showing the potential difference at the y-axis and the separation distance between the electrodes in meters at the x-axis.

Fig 4.4 Surface charge density (Cm^{-2}) versus separation distance, $d(\text{m})$ for short the circuit mode, i.e., when the electrodes are grounded and the floating potential is removed.

Fig 4.5 Electric field norm of the sliding mode TENG with showing the concentration of electric field near both the electrodes that are separated horizontally and the for the polyethylene film when the sliding distance (a) $d=0.02\text{m}$ (b) $d=0.05\text{m}$ (c) $d=0.08\text{m}$ and (d) $d=0.098\text{m}$.

Fig 4.6 Open circuit voltage versus sliding distance(mm) linear curve showing the open circuit potential difference at the y-axis and the separation distance between the electrodes in millimetres at x-axis.

Fig 4.7 Surface charge density (Cm^{-2}) versus separation distance, $d(\text{mm})$ for short the circuit mode, i.e., when the electrodes are grounded and the floating potential is removed

Fig 4.8 Electric field norm of the sliding mode TENG with showing the concentration of electric field near both the electrodes that are separated horizontally and the for the polyethylene film when the free-standing vertical contact separation, (a) $d=0.043\text{m}$ (b) $d=0.062\text{m}$ (c) $d=0.083\text{m}$ and (d) $d=0.11\text{m}$.

Fig 4.9. Open circuit voltage versus sliding distance(m) linear curve showing the open circuit potential difference at the y-axis and the separation distance between the electrodes in millimetres at the x-axis.

Fig 4.10 Surface charge density (Cm^{-2}) versus separation distance, $d(\text{m})$ for short the circuit mode, i.e., when the electrodes are grounded and the floating potential is removed.

Fig 4.11 Surface charge density versus displacement(m) when dielectric constant=1

Fig 4.12 Applications in IoT

CHAPTER 1:
INTRODUCTION

CHAPTER 1: NTRODUCTION

The field of energy harvesting has witnessed remarkable advancements in recent years, with the emergence of innovative technologies that tap into alternative sources of energy. Among these groundbreaking developments, the Triboelectric Nanogenerator (TENG) has emerged as a promising solution for harnessing mechanical energy from the surrounding environment and converting it into electrical power. The TENG technology operates based on the principle of triboelectrification, where two dissimilar materials come into contact and generate electric charges through frictional forces. This unique mechanism offers numerous opportunities for generating sustainable and self-powered systems, paving the way for a wide range of applications in various industries, including wearable electronics, Internet of Things (IoT) devices, and environmental sensors. In this introduction, we will delve into the fundamental concepts behind the triboelectric nanogenerator, explore its working principles, and highlight its potential implications in the realm of renewable energy and autonomous systems. [1-5]

Triboelectric Nanogenerator (TENG) is an innovative technology that has gained significant attention in the field of energy harvesting. It presents a unique approach to converting mechanical energy into electrical power by exploiting the phenomenon of triboelectrification. Unlike traditional energy harvesting technologies that rely on solar, wind, or thermal sources, TENG harnesses the mechanical energy available in our daily surroundings, making it a highly versatile and accessible solution. The fundamental principle behind the TENG is based on the triboelectric effect, which refers to the generation of electric charges when two dissimilar materials come into contact and then separate. During the contact, electrons are transferred between the materials, leading to the formation of positive and negative charges on their surfaces. [6,7] When the materials are separated, the built-up charges can be harvested as electricity. The construction of a TENG typically involves two essential components: a triboelectric layer and an electrode. The triboelectric layer is composed of two materials with contrasting electron affinities, creating a charge imbalance during contact and separation. The electrode, often made of a conductive material, collects the generated charges and provides an external circuit for the flow of electricity. [8]

TENG devices can take various forms depending on the specific application requirements. They can be designed as single units or as arrays of multiple units interconnected to enhance power output. The mechanical energy sources that can be utilized include human motion, vibrations, wind, water flow, and even the motion of biological systems. This versatility enables the integration of TENGs into a wide range of applications. [9] One significant advantage of TENG technology is its self-powered nature. Once the TENG is set in motion, it can generate electricity without the need for external power sources, making

it an attractive solution for autonomous systems and low-power electronic devices. Additionally, TENGs exhibit high energy conversion efficiency, fast response times, and a wide operational bandwidth. The potential applications of TENG span across various domains. In the field of wearable electronics, TENGs can be integrated into clothing or accessories to harvest energy from human body movements, providing a sustainable power source for wearable devices such as fitness trackers or smartwatches [10-12]. They can also be deployed in IoT devices, where they scavenge energy from ambient vibrations to power wireless sensors and communication modules. Furthermore, TENGs have shown promise in environmental monitoring systems, enabling the deployment of self-sustaining sensors in remote areas [13].

In conclusion, the Triboelectric Nanogenerator (TENG) technology offers a novel approach to energy harvesting by converting mechanical energy into electrical power through the triboelectrification process. With its self-powered and versatile nature, TENG has the potential to revolutionize various industries, contributing to the advancement of sustainable and autonomous systems [14,15].

There are several types of Triboelectric Nanogenerators (TENGs) that have been developed based on different designs and configurations. Each type offers unique advantages and can be tailored to specific applications. Here are some common types of TENGs:

- Contact-Separation TENG (VCS-TENG): This type of TENG consists of vertically aligned structures that undergo contact and separation. It typically involves a vertically movable structure and a fixed electrode. When the two surfaces come into contact and then separate, the triboelectric charges are generated and collected by the electrodes, resulting in electricity generation. VCS-TENGs are known for their high output power and reliability.
- Sliding-mode TENG (S-TENG): S-TENGs are designed with sliding or reciprocating motion between two surfaces. This motion creates friction and triboelectric charges, leading to electricity generation. S-TENGs can be constructed with flexible materials and are suitable for applications where sliding or rubbing motions are prevalent, such as wearable devices or touch-sensitive surfaces.
- Single-electrode TENG (SE-TENG): SE-TENGs employ a single electrode, eliminating the need for two separate electrodes. The triboelectric charges are generated on the single electrode through contact and separation with a triboelectric material. SE-TENGs offer simplicity in design and fabrication, making them cost-effective and suitable for compact devices or low-power applications.

- Hybrid TENG (H-TENG): H-TENG combines the concept of TENG with other energy harvesting technologies, such as piezoelectric or electromagnetic mechanisms. It integrates multiple energy conversion mechanisms to enhance overall energy generation. H-TENGs can harvest energy from different sources simultaneously, increasing their efficiency and adaptability to various environments.
- Rotational TENG (R-TENG): R-TENGs utilize rotational motion to generate electricity. They consist of rotating disks or wheels with triboelectric materials that make contact and separation with fixed electrodes. The continuous rotation of the disks generates a steady output of electrical energy. R-TENGs are suitable for applications where rotational motion is abundant, such as wind turbines or mechanical systems.
- Transparent TENG (T-TENG): T-TENGs are designed to be transparent, allowing them to be integrated into transparent or flexible surfaces, such as touchscreens or windows. These devices employ transparent conductive materials and can generate electricity while maintaining optical transparency, enabling their use in transparent electronic devices and smart surfaces.

These are just a few examples of the types of TENGs that have been developed. Each type offers unique characteristics and benefits, allowing for customization based on specific application requirements. The continued research and development in this field hold great potential for advancing energy harvesting technologies and promoting sustainable power generation [16].

In recent years, the rapid advancement of nanotechnology has led to the widespread use of nanostructures to address various modern-day challenges. Smart devices have become indispensable in our daily lives, from homes to industries. However, many existing devices rely on energy sources, leading to issues such as frequent battery changes, dependence on non-renewable energy, and limitations in remote areas. To overcome these limitations, the utilization of triboelectric nanogenerators (TENGs) has gained significant traction. TENGs are devices that convert mechanical energy into electrical energy [17]. They are based on two key phenomena: contact electrification and electrical induction. Contact electrification occurs when objects come into close proximity, inducing electric charges on their surfaces. Electrical induction, on the other hand, refers to the charging of an electrical conductor upon contact with a charged body. These phenomena enable TENGs to exhibit fast response times, compact and flexible structures, high efficiency, and low detection limits. TENGs operate in three different modes: contact mode, sliding mode, and free-standing mode. In the contact mode, the triboelectric layers are connected to a mechanical source and a lead wire. In the sliding mode, the top layer of the generator is horizontally movable, allowing for variable distance between the ends of the top and bottom layers. The free-standing

mode consists of three layers, with the top layer separated by a distance from the two layers below, which lie on the same level [18-20].

Wearable devices based on TENGs typically utilize the contact and sliding modes. However, for devices that require versatility and the ability to function with arbitrary objects, the free-standing mode of the triboelectric generator is crucial. By employing multiple layers connected with electrodes and inducing opposite static charges through external mechanical factors, the triboelectric nanogenerator produces high voltage with low current and high intrinsic impedance [21].

The first demonstration of a free-standing triboelectric nanogenerator was conducted by Sihong Wang in 2014. Since then, triboelectric nanogenerators have been extensively studied and utilized as energy harvesting systems based on sustainable resources. They find applications in various fields, including sensing technologies, Internet of Things (IoT), and air filtration. Overall, triboelectric nanogenerators offer a promising solution for harnessing energy from mechanical sources, providing an efficient and sustainable approach to power generation and energy harvesting [22].

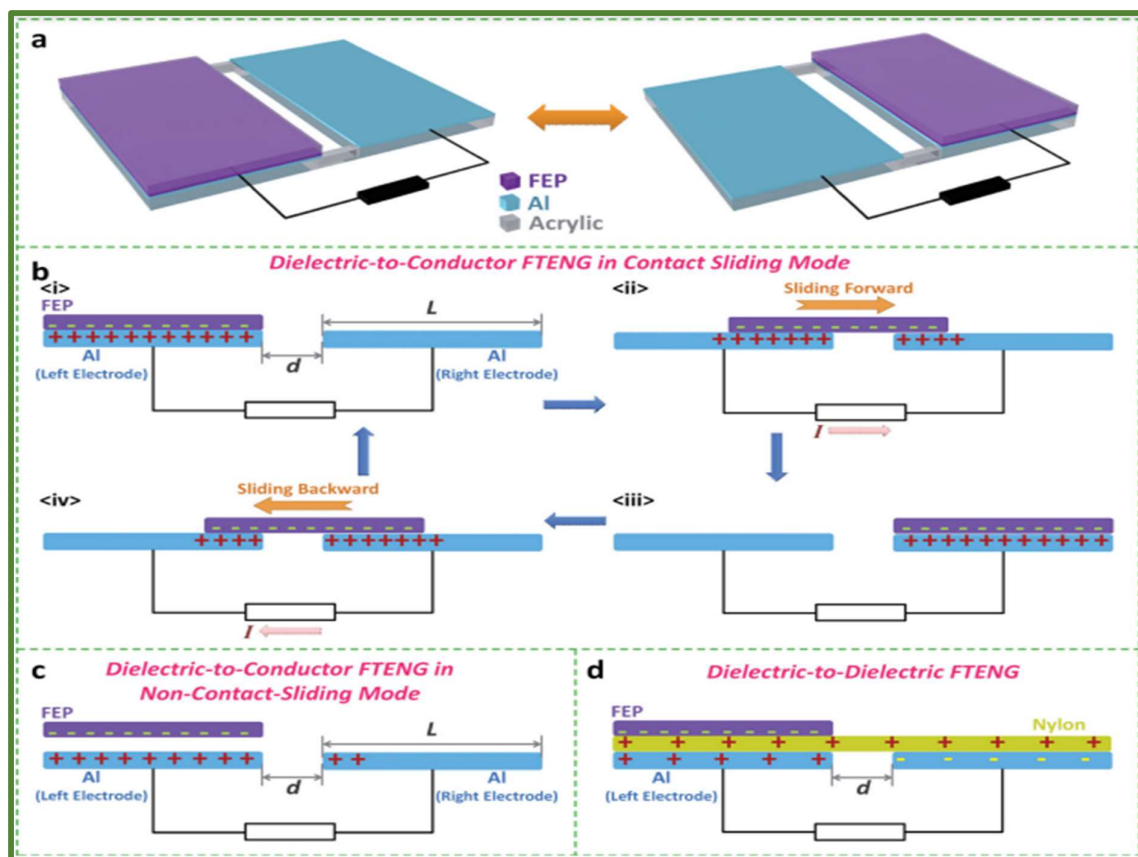


Figure 1. Device structure, basic operations and working principles of the freestanding-triboelectric-layer based nanogenerator (FTENG). (a) Typical device structure of a conductor-to-dielectric FTENG. (b) Schematic working principle of a conductor-to-dielectric FTENG in contact sliding mode. (c) Schematic diagram of a conductor-to-dielectric FTENG in non-contact sliding mode. (d) Schematic diagram of a dielectric-to-dielectric FTENG.

The traditional triboelectric generators, such as the Van de Graaff generator and Wimshurst machine, were invented in the late 19th and early 20th centuries. These generators were designed to generate static electricity through contact charges and accumulate large charge values using corona discharge. They produced high voltage output with no significant current but were bulky and not suitable for compact devices like smartwatches or sensors.

To address this limitation, triboelectric nanogenerators (TENGs) were developed. TENGs can operate in a self-powered mode with a constant capacitance and fixed electric field. In this paper, the three modes of TENGs, namely contact mode, sliding mode, and free-standing mode, are designed, analysed, and their efficiencies are calculated and compared [23].

The TENG in this study features positive electrodes made of Al_2O_3 , chosen for its stability and charge conductivity, while the negative electrode is made of polyethylene, acting as the dielectric material. The open-source and short-circuit voltages of the nanogenerator are shown to vary with the contact separation between the layers, with separation values ranging from a few millimetres and voltage values given in volts. The surface charge density for the short-circuited nanogenerator is also calculated and shown to vary with the separation between the layers [24]. The applications of TENGs in smart devices are demonstrated, particularly in smart sensors based on contact-based TENGs, with their efficiency calculated. The paper also showcases the use of TENG-based sensors in common applications and energy harvesting. TENGs are self-powered devices that convert mechanical energy into electrical energy, making them suitable for various devices to detect changes in electric current due to motion, with a calculated maximum sensitivity of approximately 105 Vm^{-1} [25].

CHAPTER 2:
STRUCTURAL DESIGNING
AND
MODELLING

CHAPTER 2: STRUCTURAL AND DESIGN ANALYSIS

The proposed design of the TENG aims to induce charges and generate a self-generated electric field by applying an external source of electricity. This design focuses on vertical separation-based TENGs, where two layers are stacked with a separation of millimetres.

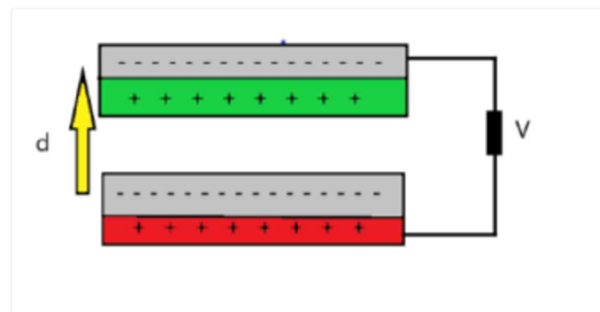


Fig 2.1(a) Contact separation TENG

Figure 2.1(a) illustrates the contact separation mode of the TENG, where an external voltage (V) leads to the induction of opposite charges on surfaces close to each other and similar charges on opposing surfaces. This arrangement facilitates greater variation in separation, resulting in increased deflection in both open-circuit and short-circuit voltages. The vertical separation-based TENG design offers potential applications in energy harvesting and power generation. By optimizing the design parameters, such as the separation distance, the performance and efficiency of TENG systems can be enhanced. The findings of this study contribute to the advancement of TENG technology and its application in various fields.

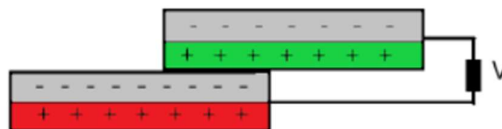


Fig 2.1(b) Contact sliding TENG

While vertical separation is effective in calculating the frequency of the TENG, it may not be efficient for amplitude calculation. To address this, two other modes of TENG have been developed. The sliding mode TENG, depicted in Figure 2.1(b), features a horizontal separation between the ends of two

electrodes that are stacked in contact. In this mode, an applied voltage varies the horizontal distance, referred to as the sliding distance. By observing the variations in open-circuit and short-circuit voltages corresponding to the sliding distance, the amplitude of the TENG output can be determined. The sliding mode TENG offers an alternative approach for amplitude calculation, complementing the vertical separation mode. The findings of this study contribute to expanding the understanding and applications of TENG technology in energy harvesting and power generation systems.

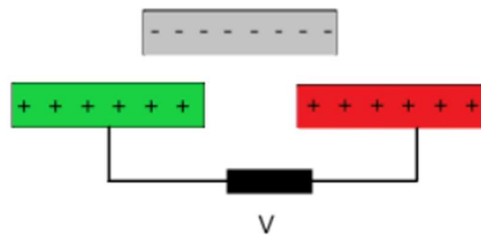


Fig 2.1(c) Freestanding TENG

The most recent and highly efficient mode of TENG is the free-standing mode, depicted in Figure 2.1(c). In this mode, two electrodes are positioned in the same plane, while a movable electrode lies above them at a constant vertical separation and slides between the underlying layers. The free-standing mode offers a superior energy harvesting structure that is electrode-free, ensuring higher stability. It is suitable for capturing energy from arbitrary moving objects and finds extensive applications in the Internet of Things (IoT) and power harvesting domains. The unique and stable structure of the free-standing TENG makes it a popular choice for various practical implementations. This paper explores the design, performance, and potential applications of the free-standing TENG, contributing to advancements in energy harvesting and IoT technologies.

In our model, the electrodes are constructed using Alumina or aluminium oxide due to their stable and highly conductive properties. The upper layer comprises a Polyethylene film with a thickness of approximately $50\mu\text{m}$. Polyethylene is chosen as the material for its negative polarity in triboelectric generation. The Alumina electrodes are positively charged, while the Polyethylene is negatively charged to facilitate the triboelectric phenomenon. These materials are stacked together using acrylic sheets.

For the contact mode, the initial separation (d) between the electrodes is set at approximately 0.001m and varied up to 0.020m . In the sliding mode, the horizontal sliding distance is initially set at 1mm and then varied up to 100mm , while keeping the vertical separation (d) between the electrodes

constant. In the free-standing mode, the initial separation is set to 0.01m and varied up to 0.05m. For each separation value in all the modes of TENG, the corresponding open-source voltages and short-circuit surface charge densities are recorded. The variations in these parameters are observed for different separation values to analyse the performance of the TENG system. By conducting these experiments and collecting data, we can gain insights into the behaviour and characteristics of the TENG system in different modes. This information is valuable for optimizing the design and understanding the performance of TENG in various applications [7].

Once the parameters for the contact, sliding, and free-standing modes have been defined, the geometric structures for each mode are created by positioning rectangles in the software. The obtained geometry of the TENGs is depicted in Figure (2.2). The chosen parameters for this model are as follows:

- Length of Al_2O_3 electrodes: 0.064m
- Thickness of Al_2O_3 electrodes: 10^{-5}m
- Length of Polyethylene dielectric: 0.064m
- Thickness of Polyethylene dielectric: 10^{-4}m
- Separation distance (d): 0.01006m

These specific parameter values ensure the desired geometry and dimensions of the TENG structures. They are crucial for accurately simulating and analysing the performance of the TENG system in each mode.

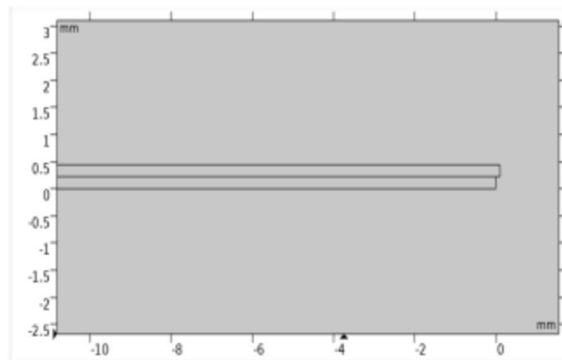


Fig 2.2 (a) Geometrical model for contact mode TENG

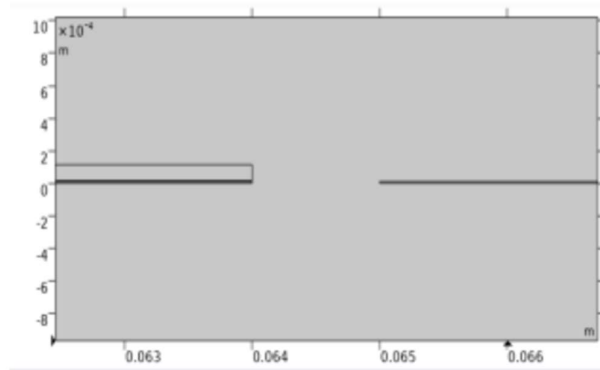


Fig 2.2 (b) Geometrical model for sliding mode TENG

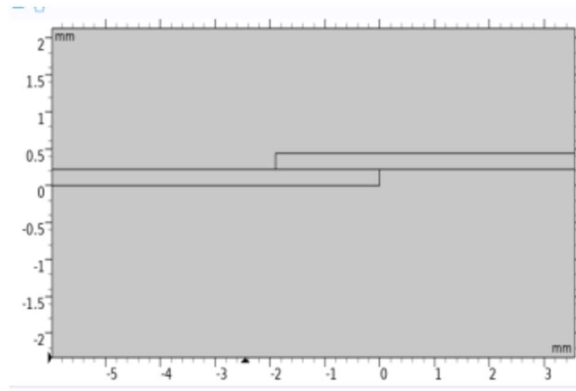


Fig 2.2 (c) Geometrical model for freestanding mode TENG

The designed geometry for the TENG modes with stacked layers with the top and bottom layers being Al_2O_3 electrodes and in the middle being the thin nanofilm of polyethylene. Fig2.2(a) Layers of electrodes for contact mode with contact separation being of the order of a few millimetres Fig 2.2 (b) The designed structure for the sliding layers of the sliding mode TENG. Fig 2.2 (c) Free-standing mode designed structure for TENG with two electrodes below and single electrode above them and the polyethylene film between the electrodes.

CHAPTER 3:
DESIGN ANALYSIS
OF
SOFTWARE USED
(COMSOL MULTIPHYSICS)

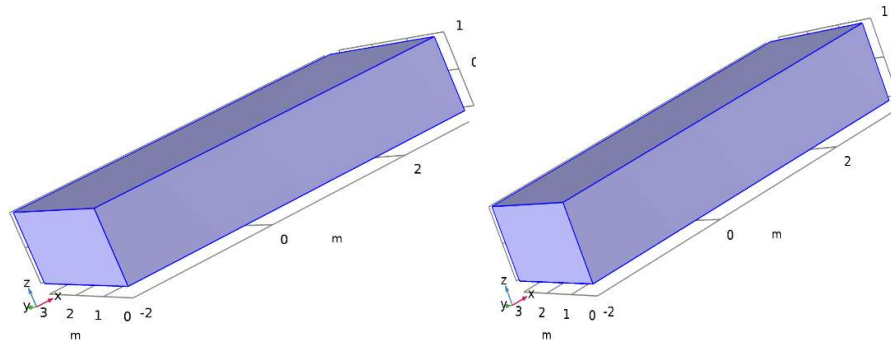


Fig 3.1 Material

Materials used:

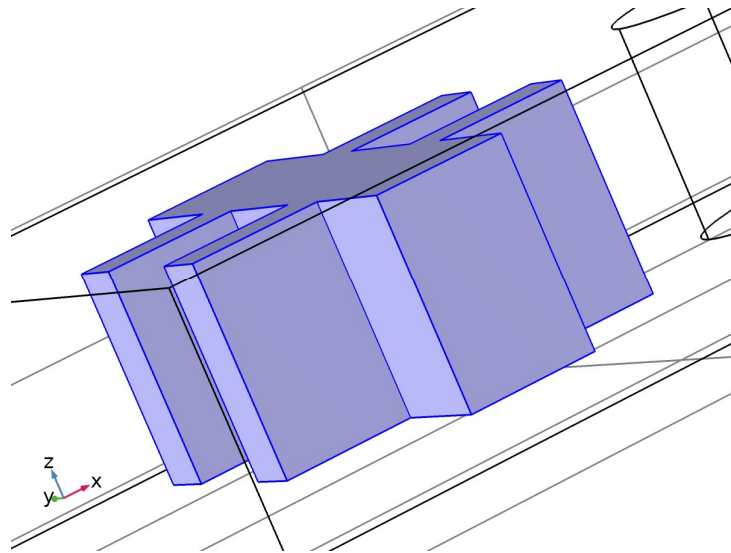


Fig 3.2 Material Parameters

Table 3.1 Variables

Name	Expression	Unit	Description	Selection
es.ny	ny		Normal vector, y component	Boundaries 6–37
es.nz	nz		Normal vector, z component	Boundaries 6–37
es.nx	dnx		Normal vector, x component	Boundaries 1–5, 38
es.ny	dny		Normal vector, y component	Boundaries 1–5, 38
es.nz	dnz		Normal vector, z component	Boundaries 1–5, 38
es.nmeshx	nxmesh		Mesh normal vector, x component	Boundaries 6–37
es.nmeshy	nymesh		Mesh normal vector, y component	Boundaries 6–37
es.nmeshz	nzmesh		Mesh normal vector, z component	Boundaries 6–37
es.nmeshx	dnxmesh		Mesh normal vector, x component	Boundaries 1–5, 38
es.l_sXX	$(\text{spatial.invF11} * (\text{spatial.invF11} * \text{es.l_sxx} + \text{spatial.invF21} * \text{es.l_syx} + \text{spatial.invF31} * \text{es.l_szx}) + \text{spatial.invF21} * (\text{spatial.invF11} * \text{es.l_sxy} + \text{spatial.invF21} * \text{es.l_syy} + \text{spatial.invF31} * \text{es.l_szy}) + \text{spatial.invF31} * (\text{spatial.invF11} * \text{es.l_sxz} + \text{spatial.invF21} * \text{es.l_syz} + \text{spatial.invF31} * \text{es.l_szz})) * \text{spatial.detF}$	1	Spatial identity matrix, material frame, XX component	Domains 1–3
es.l_sYX	$(\text{spatial.invF11} * (\text{spatial.invF12} * \text{es.l_sxx} + \text{spatial.invF22} * \text{es.l_syx} + \text{spatial.invF32} * \text{es.l_szx}) + \text{spatial.invF21} * (\text{spatial.invF12} * \text{es.l_sxy} + \text{spatial.invF22} * \text{es.l_syy} + \text{spatial.invF32} * \text{es.l_szy}) + \text{spatial.invF31} * (\text{spatial.invF12} * \text{es.l_sxz} + \text{spatial.invF22} * \text{es.l_syz} + \text{spatial.invF32} * \text{es.l_szz})) * \text{spatial.detF}$	1	Spatial identity matrix, material frame, YX component	Domains 1–3

Name	Expression	Unit	Description	Selection
			downside, z component	
es.l_sXX	$(\text{spatial.invF11} * (\text{spatial.invF11} * \text{es.l_sxx} + \text{spatial.invF21} * \text{es.l_syx} + \text{spatial.invF31} * \text{es.l_szx}) + \text{spatial.invF21} * (\text{spatial.invF11} * \text{es.l_sxy} + \text{spatial.invF21} * \text{es.l_syy} + \text{spatial.invF31} * \text{es.l_szy}) + \text{spatial.invF31} * (\text{spatial.invF11} * \text{es.l_sxz} + \text{spatial.invF21} * \text{es.l_syz} + \text{spatial.invF31} * \text{es.l_szz})) * \text{spatial.detF}$	1	Spatial identity matrix, material frame, XX component	Domains 1–3
es.l_sYX	$(\text{spatial.invF11} * (\text{spatial.invF12} * \text{es.l_sxx} + \text{spatial.invF22} * \text{es.l_syx} + \text{spatial.invF32} * \text{es.l_szx}) + \text{spatial.invF21} * (\text{spatial.invF12} * \text{es.l_sxy} + \text{spatial.invF22} * \text{es.l_syy} + \text{spatial.invF32} * \text{es.l_szy}) + \text{spatial.invF31} * (\text{spatial.invF12} * \text{es.l_sxz} + \text{spatial.invF22} * \text{es.l_syz} + \text{spatial.invF32} * \text{es.l_szz})) * \text{spatial.detF}$	1	Spatial identity matrix, material frame, YX component	Domains 1–3
es.l_sZX	$(\text{spatial.invF11} * (\text{spatial.invF13} * \text{es.l_sxx} + \text{spatial.invF23} * \text{es.l_syx} + \text{spatial.invF33} * \text{es.l_szx}) + \text{spatial.invF21} * (\text{spatial.invF13} * \text{es.l_sxy} + \text{spatial.invF23} * \text{es.l_syy} + \text{spatial.invF33} * \text{es.l_szy}) + \text{spatial.invF31} * (\text{spatial.invF13} * \text{es.l_sxz} + \text{spatial.invF23} * \text{es.l_syz} + \text{spatial.invF33} * \text{es.l_szz})) * \text{spatial.detF}$	1	Spatial identity matrix, material frame, ZX component	Domains 1–3

Charge Conservation 1 (Fig 3.3)

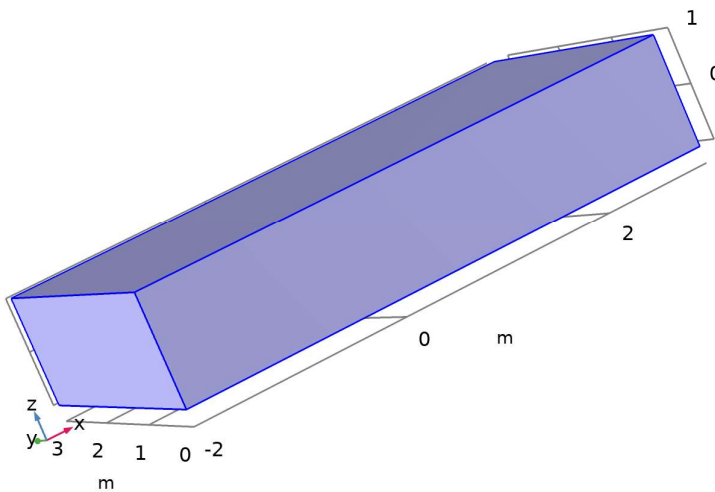


Table 3.2 Variables

Name	Expression	Unit	Description	Selection	Details
es.nD	0	C/m ²	Surface charge density	Boundaries 1–38	+ operation
es.epsilonrx	material.epsilonr11	1	Relative permittivity, xx component	Domains 1–3	Meta
es.epsilonryx	material.epsilonr21	1	Relative permittivity, <u>yx</u> component	Domains 1–3	Meta
es.epsilonrxz	material.epsilonr31	1	Relative permittivity, <u>zx</u> component	Domains 1–3	Meta
es.epsilonrxy	material.epsilonr12	1	Relative permittivity, <u>xy</u> component	Domains 1–3	Meta
es.epsilonryy	material.epsilonr22	1	Relative permittivity, <u>yy</u> component	Domains 1–3	Meta
es.epsilonrzy	material.epsilonr32	1	Relative permittivity, <u>zy</u> component	Domains 1–3	Meta
es.epsilonrxz	material.epsilonr13	1	Relative permittivity, <u>xz</u> component	Domains 1–3	Meta
es.epsilonryz	material.epsilonr23	1	Relative permittivity, <u>yz</u> component	Domains 1–3	Meta

Name	Expression	Unit	Description	Selection	Details
	$\text{silon0_const} * \text{es.l_szz} * \text{es.Ez} + \text{es.Pz} + \text{es.Pez}$				
es.Px	$\text{epsilon0_const} * (\text{es.chixx} * \text{es.Ex} + \text{es.chixy} * \text{es.Ey} + \text{es.chixz} * \text{es.Ez})$	C/m ²	Polarization, x component	Domains 1–3	
es.Py	$\text{epsilon0_const} * (\text{es.chiyx} * \text{es.Ex} + \text{es.chiyy} * \text{es.Ey} + \text{es.chiyz} * \text{es.Ez})$	C/m ²	Polarization, y component	Domains 1–3	
es.Pz	$\text{epsilon0_const} * (\text{es.chizx} * \text{es.Ex} + \text{es.chizy} * \text{es.Ey} + \text{es.chizz} * \text{es.Ez})$	C/m ²	Polarization, z component	Domains 1–3	
es.normD	$\text{sqrt}(\text{realdot}(\text{es.Dx}, \text{es.Dx}) + \text{realdot}(\text{es.Dy}, \text{es.Dy}) + \text{realdot}(\text{es.Dz}, \text{es.Dz}))$	C/m ²	Electric displacement field norm	Domains 1–3	
es.normP	$\text{sqrt}(\text{realdot}(\text{es.Px}, \text{es.Px}) + \text{realdot}(\text{es.Py}, \text{es.Py}) + \text{realdot}(\text{es.Pz}, \text{es.Pz}))$	C/m ²	Polarization norm	Domains 1–3	
es.Pex	0	C/m ²	Polarization contribution, x component	Domains 1–3	+ operation
es.Pey	0	C/m ²	Polarization contribution, y component	Domains 1–3	+ operation

Weak Expressions

Weak expression	Integration order	Integration frame	Selection
- (es.Dx*test(Vx)+es.Dy*test(Vy)+es.Dz*test(Vz))*es.d	4	Spatial	Domains 1-3

Shape functions

Name	Shape function	Unit	Description	Shape frame	Selection	Details
V	Lagrange (Quadratic)	V	Electric potential	Spatial	No boundaries	Slit
V	Lagrange (Quadratic)	V	Electric potential	Material	No boundaries	Slit
V	Lagrange (Quadratic)	V	Electric potential	Geometry	No boundaries	Slit
V	Lagrange (Quadratic)	V	Electric potential	Mesh	No boundaries	Slit

Name	Shape function	Unit	Description	Shape frame	Selection	Details
V	Lagrange (Quadratic)	V	Electric potential	Spatial	No boundaries	Slit
V	Lagrange (Quadratic)	V	Electric potential	Material	No boundaries	Slit
V	Lagrange (Quadratic)	V	Electric potential	Geometry	No boundaries	Slit
V	Lagrange (Quadratic)	V	Electric potential	Mesh	No boundaries	Slit

MESH

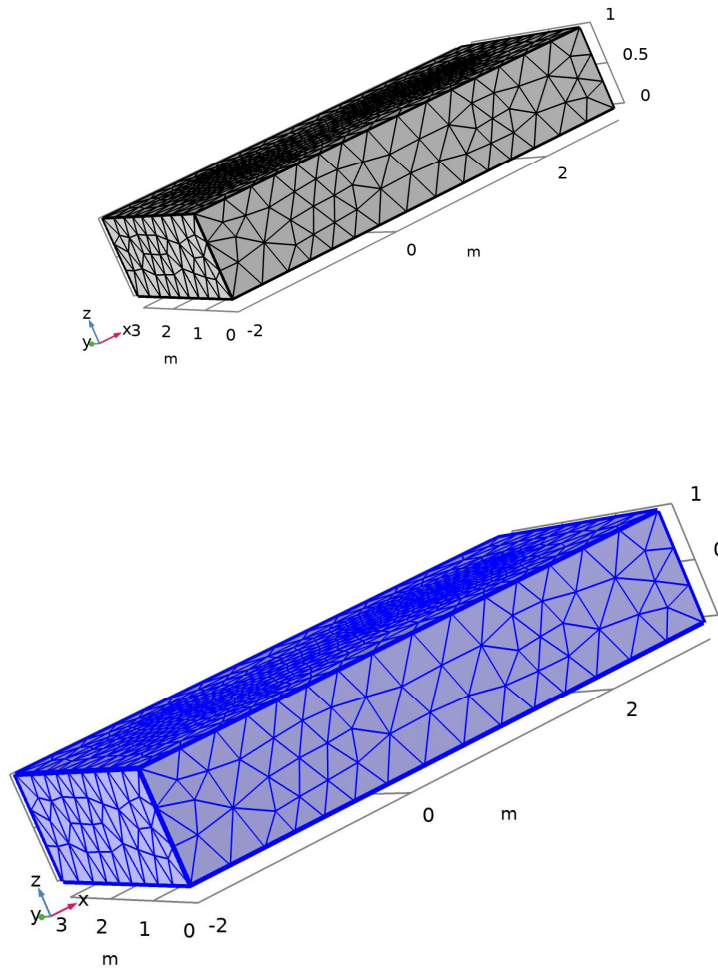


Fig 3.4 Mesh Model

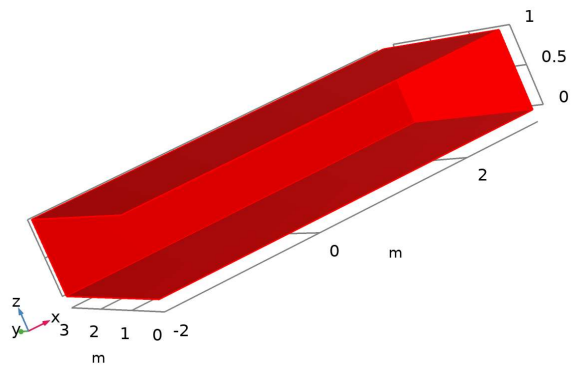


Fig 3.5 Dataset: Study 1/Solution 1

Surface: Surface charge density (pC/m^2)
 Streamline: Electric field Streamline Color: Electric field norm (V/m)

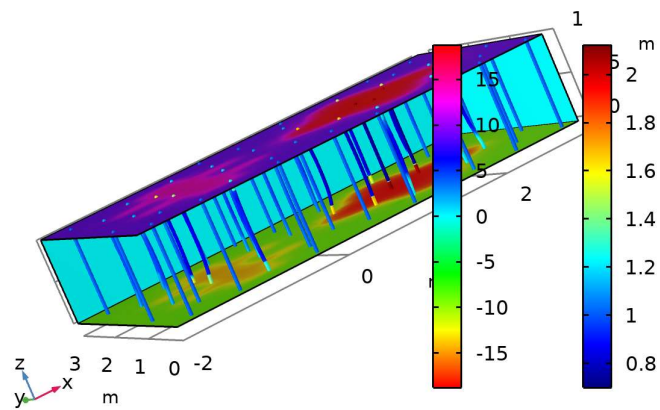


Fig 3.6 Surface: Surface charge density (pC/m^2) Streamline: Electric field Streamline Color: Electric field norm (V/m)

CHAPTER 4:
RESULTS
AND
SIMULATION

Chapter 4: Contact mode TENG

After designing the geometry of the contact mode, the materials are selected and the voltage is applied at the electrodes with a constant contact separation of 0.01m. After application of the voltage to the electrodes, there is free potential applied to each surface and thus, there is a generation of the electric field between the electrodes and in the external surrounding medium which is taken as air. The electric field norm is run for the stationary frequency mode analysis of the contact mode TENG model, then, the obtained model showing the distribution of electric field is as shown in figure 4.1. The figure basically shows the surface electric potential lying between the electrodes when the separation is changed from 0.06 to 0.013 meters. The electric field cloud is increasing with an increase in contact separation which is basically shown by the blue and red coloured fields taken. The positive and the negative charges are thus induced and when there is a short circuit applied the induced charges generate a surface charge density which also depends on the contact separation as is further shown in the curves.

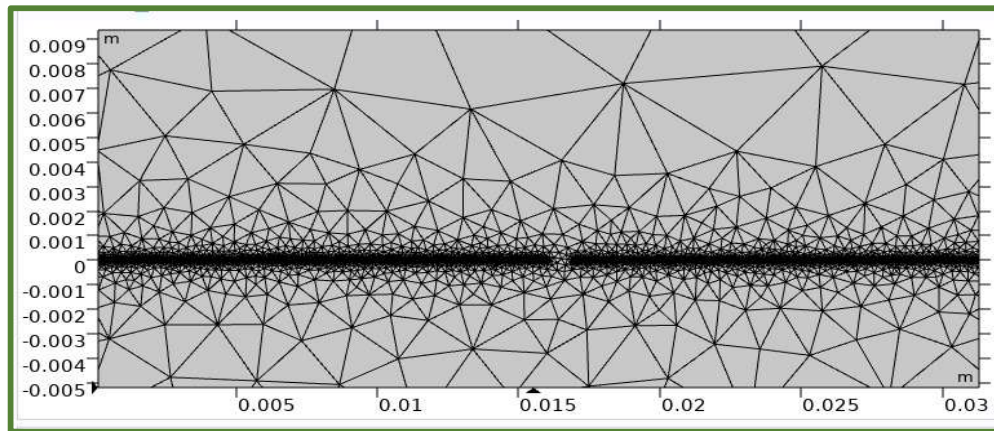


Fig 4.1. The mesh structure for the TENG geometry showing the minute details of the electrodes and their separation.

The variation in the contact mode separation, d yields an increment in open circuit potential difference (V), which is high from distance 0 to 0.015m and then a slow increment is there with distance. This variation is seen in figure 4.2. The open-circuit voltage can be calculated by the following equation [6],

$$V = \frac{\sigma d}{\epsilon_0} \quad (1)$$

Where, σ is the triboelectric charge density which is predefined and ϵ_0 is the permittivity of free space.

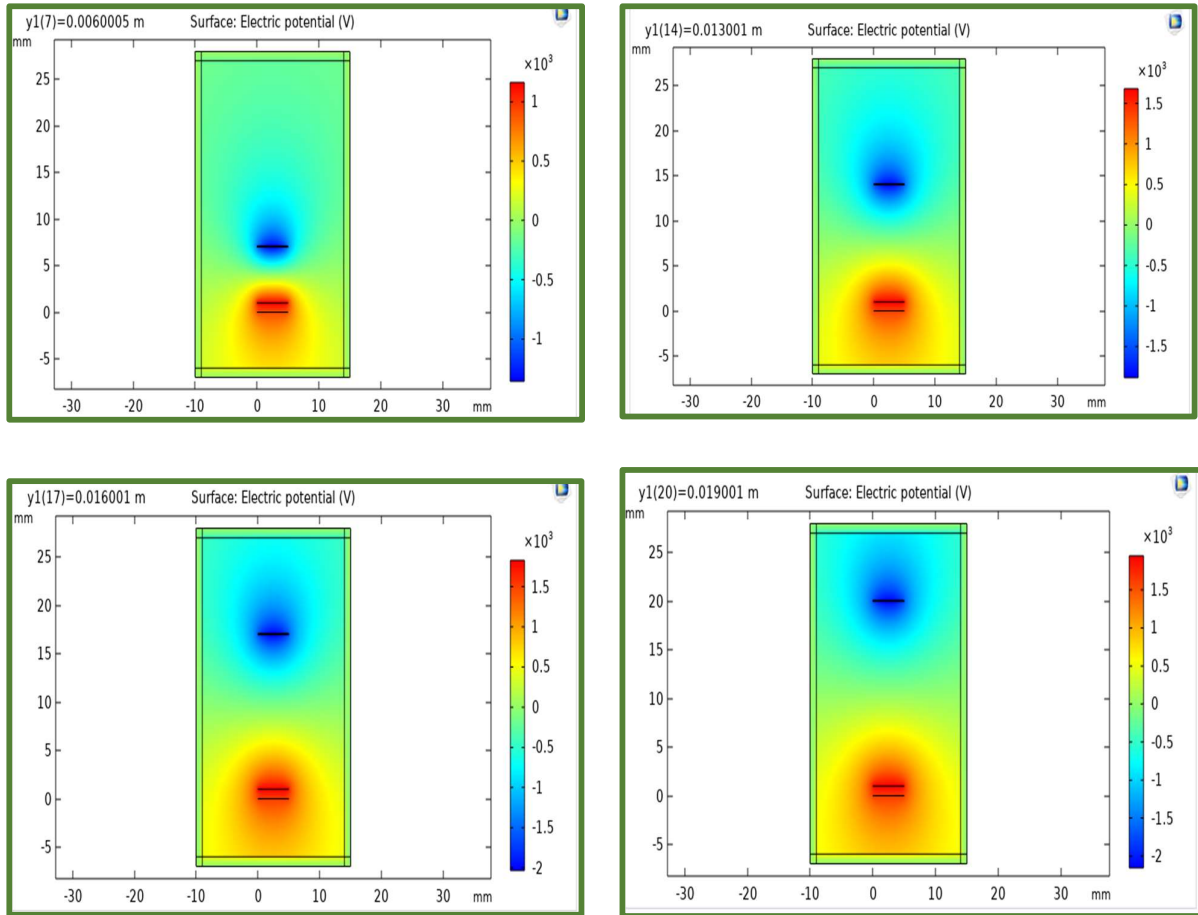


Fig 4.2 Electric field norm of contact mode TENG showing the distribution of the electric field when the electrodes that are positive and negative are close to each other. With the Polyethylene layer being negative and the Al_2O_3 layers being positive. The distance of separation for (a) $d=0.006\text{m}$ (b) $d=0.013\text{m}$ (c) $d=0.016\text{m}$ and (d) $d=0.019\text{m}$.

From figure 4.3, it is observed that after applying the free potentials to the surfaces of the electrodes there is a generation of the open-source voltage at a constant contact separation. When the contact separation is further increased, there is a linear increase observed in the value of open-source voltage up to 0.005m . However, when the distance is further increased up to 0.020m , the rise in the open-source voltage is less and more of a constant or slightly rising curve is achieved.

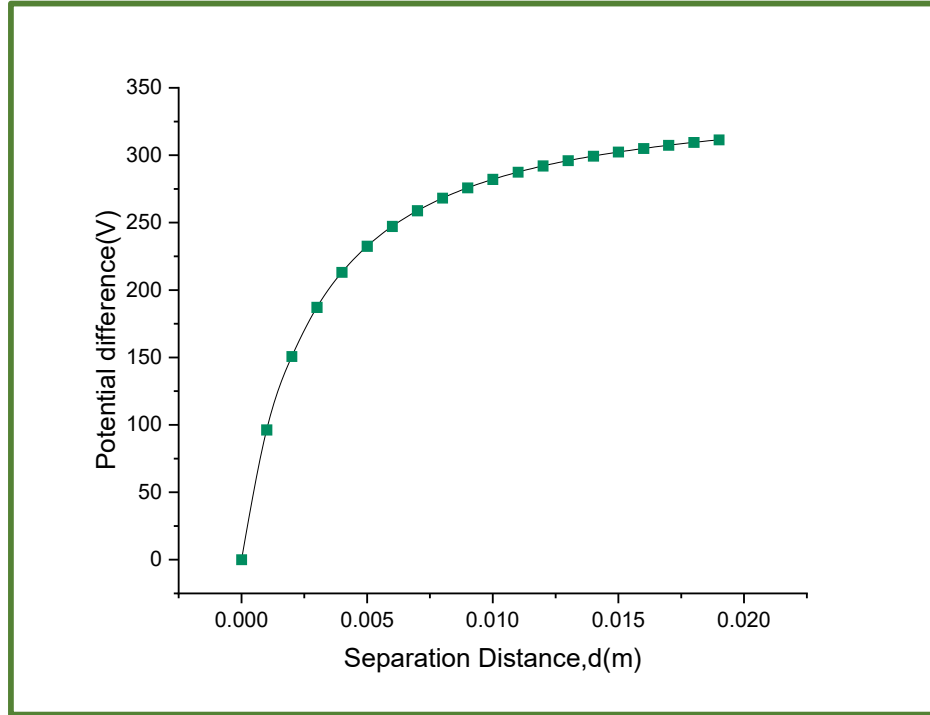


Fig 4.3 Open circuit voltage versus contact separation distance curve showing the potential difference at the y-axis and the separation distance between the electrodes in meters at the x-axis.

The surface charge density is calculated by using the equation [7],

$$\sigma_m = \frac{BP\varepsilon_0(d + \varepsilon_r x)}{(\ln(Px) + C)d} \quad (2)$$

where B and C are constants defined by the composition of material and pressure, P is atmospheric pressure of 101Pa, ε_0 , and ε_r are the permittivity of free space ($8.85 \times 10^{-12} \text{ Fm}^{-1}$) and relative permittivity of the material medium, respectively. From figure 4.4, Therefore, the surface charged density is almost constant when the separation of the Al_2O_3 electrodes and the polyethylene thin film is from 0.010 to 0.020 meters. Whereas when the separation is of the order of a few millimetres there is a steep increase observed in the surface charge density.

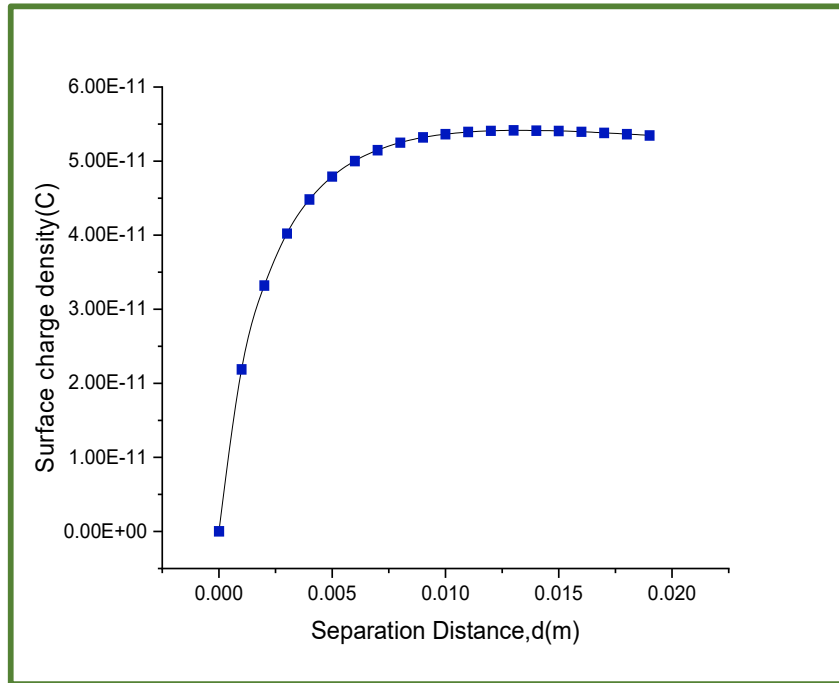


Fig 4.4 Surface charge density (Cm^{-2}) versus separation distance, d(m) for short the circuit mode, i.e., when the electrodes are grounded and the floating potential is removed.

Sliding Mode TENG

After fabricating the sliding mode geometrically, the materials are selected and the voltage is applied at the electrodes with a constant contact separation of 20.1mm. After application of the voltage to the electrodes, there is free potential applied to each surface and thus, there is a generation of the electric field between the electrodes and in the external surrounding medium which is taken as air. The electric field norm is run for the stationary frequency mode analysis of the sliding mode TENG model, then, the obtained model showing the distribution of electric field is as shown in figure 4.5. The figure basically shows the surface electric potential lying between the electrodes when the separation is changed from 20.1 to 98.1 millimetres. The electric field cloud is increasing horizontally with an increase in sliding separation which is basically shown by the blue, orange, and yellow-coloured fields taken. The positive and the negative charges are thus induced and when there is a short circuit applied the induced charges generate a surface charge density which also depends on the contact separation as is further shown in the curves.

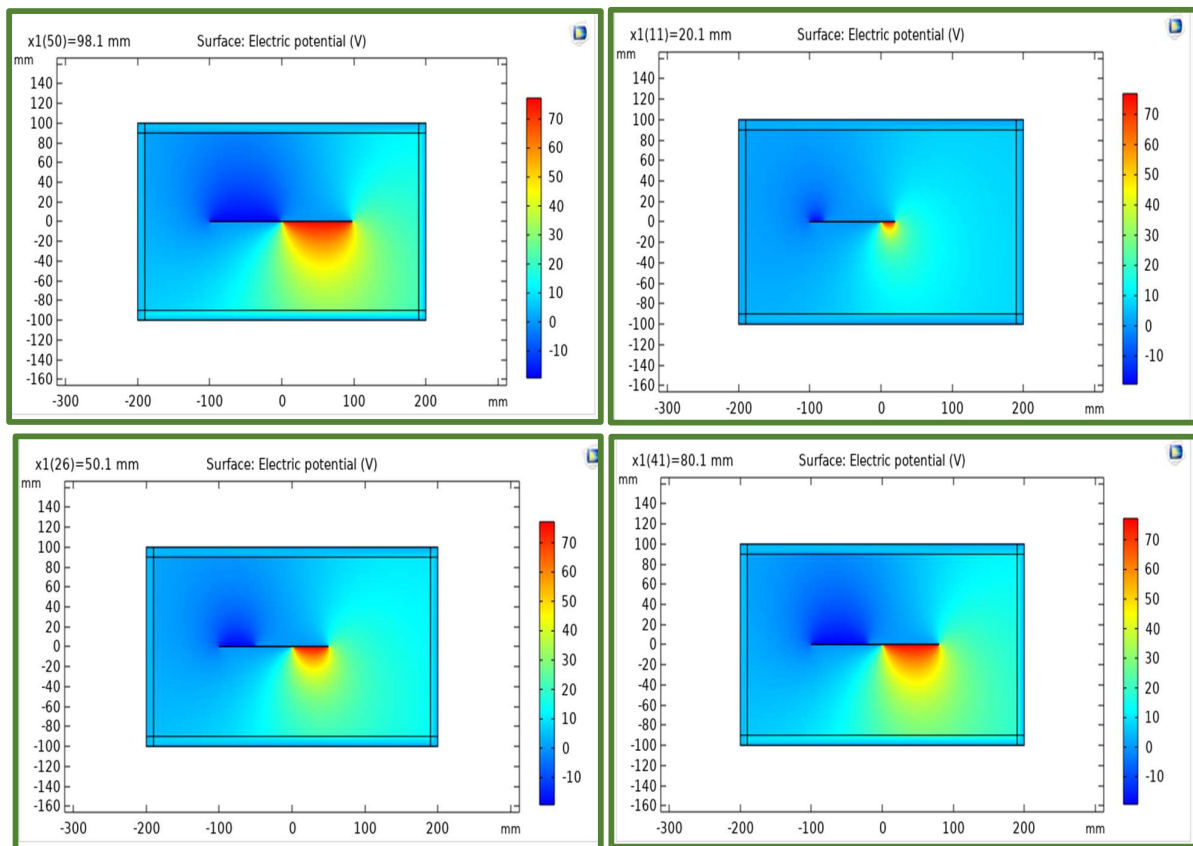


Fig 4.5. Electric field norm of the sliding mode TENG with showing the concentration of electric field near both the electrodes that are separated horizontally and the for the polyethylene film when the sliding distance (a)d=0.02m (b)d=0.05m (c) d=0.08m and (d) d=0.098m.

The variation in the sliding mode separation, d yields a constant increment in open circuit potential difference (V), calculated by equation (1) which can be seen in figure 4.6. From figure 4.6, it is observed that after applying the free potentials to the surfaces of the electrodes there is a generation of the open-source voltage at a constant contact separation. When the contact separation is further increased, there is a total linear increase observed in the value of open-source voltage up to 100mm. The open-source voltage of the sliding mode of the TENG is directly proportional to the sliding distance.

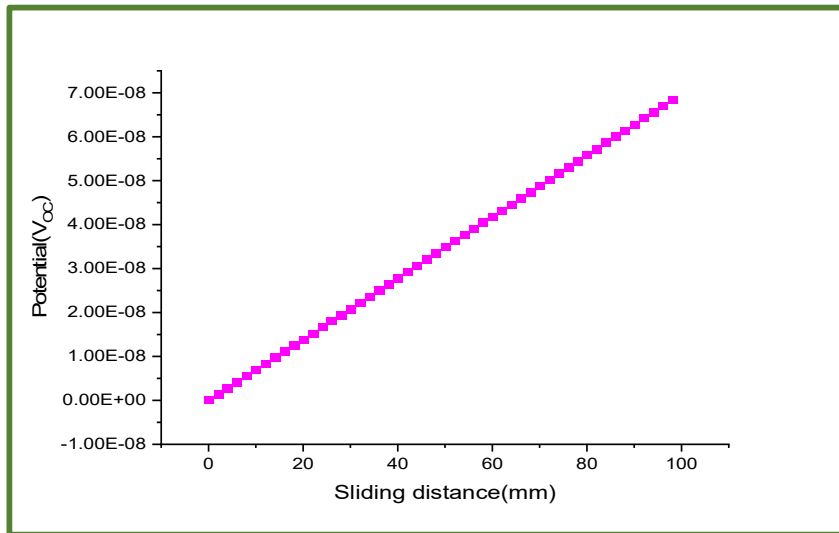


Fig 4.6 Open circuit voltage versus sliding distance(mm) linear curve showing the open circuit potential difference at the y-axis and the separation distance between the electrodes in millimetres at x-axis.

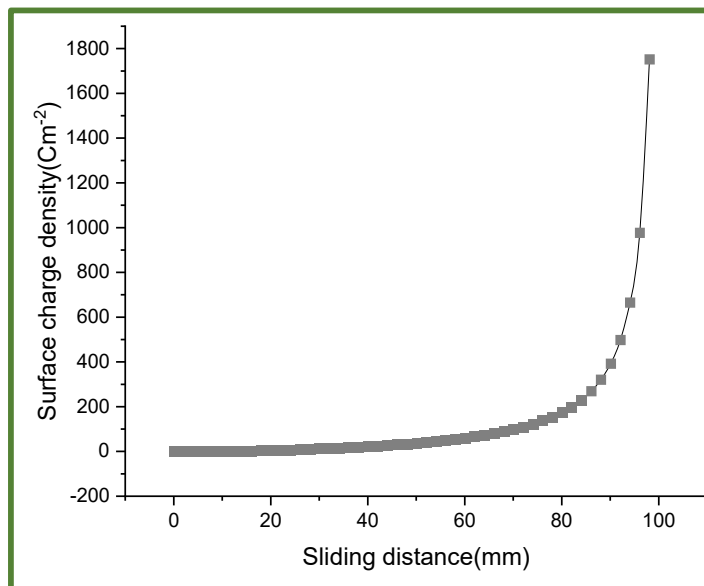


Fig 4.7 Surface charge density (Cm^{-2}) versus separation distance, d (mm) for short the circuit mode, i.e., when the electrodes are grounded and the floating potential is removed

The variation in surface charge density of TENG as calculated by equation (2) is shown in figure 4.7. Therefore, the surface charge density is almost constant when the separation of the Al_2O_3 electrodes and the polyethylene thin film is from 0 to 60 millimetres. Whereas when the separation is of the order of 60 to 100 millimetres there is a steep increase observed in the surface charge density.

Freestanding Mode TENG

The designing of the free-standing mode after the materials are selected and the voltage is applied at the electrodes with a constant contact separation of 0.042975mm. After application of the voltage to the electrodes, there is free potential applied to each surface and thus, there is a generation of the electric field between the electrodes and in the external surrounding medium which is taken as air. The electric field norm is run for the stationary frequency mode analysis of the free-standing mode TENG model, then, the obtained model showing the distribution of electric field is as shown in figure 4.8. The figure basically shows the surface electric potential lying between the electrodes when the separation is changed from 0.04 to 0.11 meters. The electric field cloud is increasing horizontally with an increase in sliding separation which is basically shown by the blue, orange, green, and yellow-colored fields taken. The positive and the negative charges are thus induced and when there is a short circuit applied the induced charges generate a surface charge density which also depends on the contact separation as is further shown in the curves.

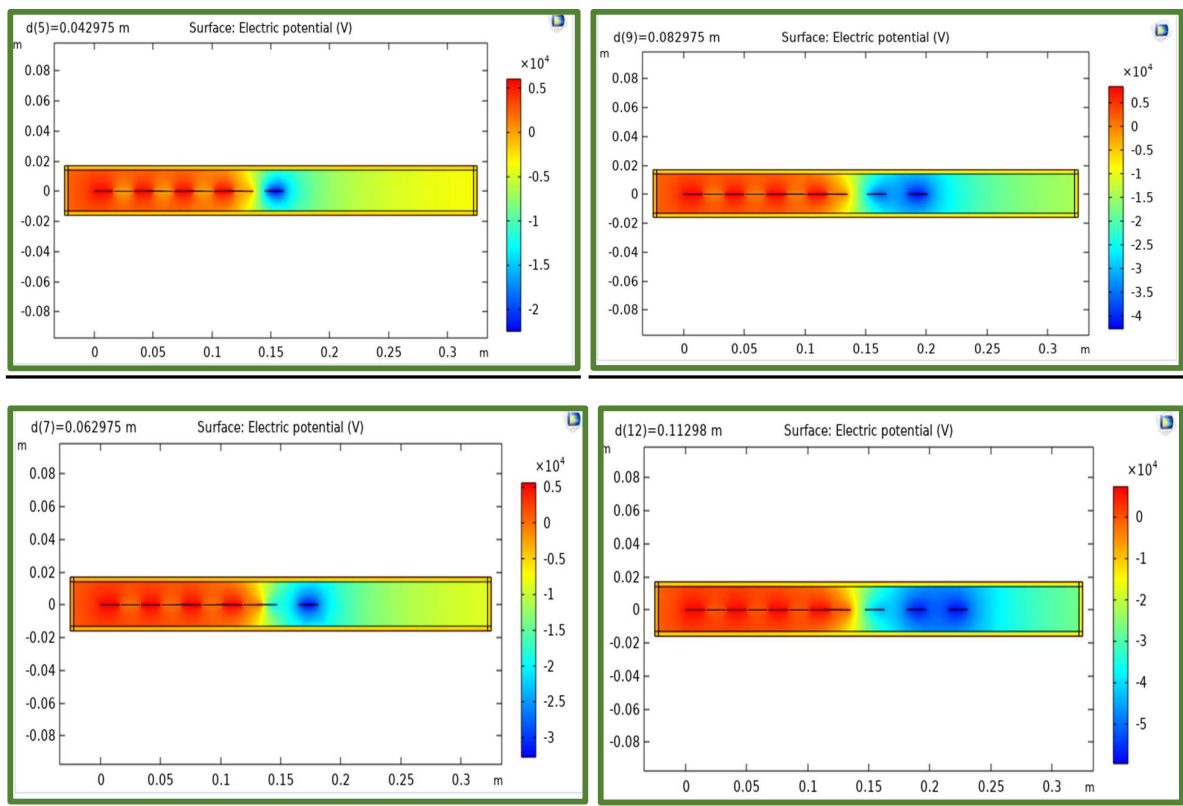


Fig 4.8 Electric field norm of the sliding mode TENG with showing the concentration of electric field near both the electrodes that are separated horizontally and the for the polyethylene film when the free-standing vertical contact separation, (a) $d=0.043$ m (b) $d=0.062$ m (c) $d=0.083$ m and (d) $d=0.11$ m.

The variation in the freestanding mode separation, d yields a zig-zag pattern in variation of open circuit potential difference (V), calculated by equation (1), which can be seen in figure 4.9. The increase in the open-circuit voltage is observed when the distance is varied from 0 to 0.02 meters while there is a decrease in the open-circuit voltage from 0.02 to 0.03 meters and then, again, an increase in the open-source voltage is observed from 0.035 to 0.04 meters of contact separation followed by a decrease at the last 0.045-0.05 meters.

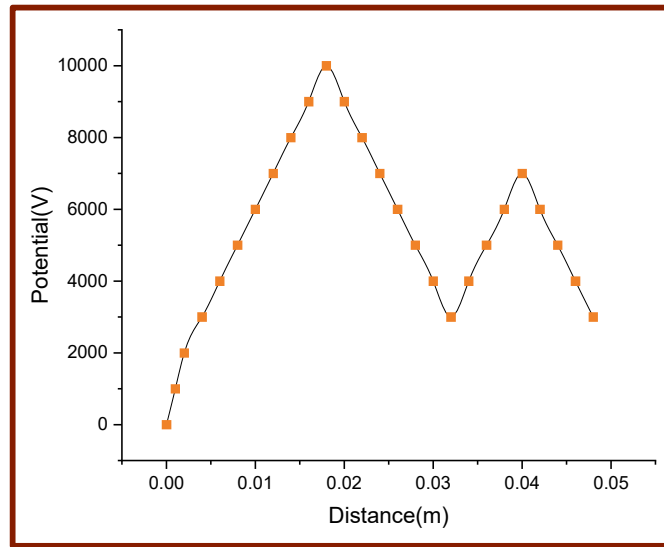


Fig 4.9. Open circuit voltage versus sliding distance(m) linear curve showing the open circuit potential difference at the y-axis and the separation distance between the electrodes in millimetres at the x-axis.

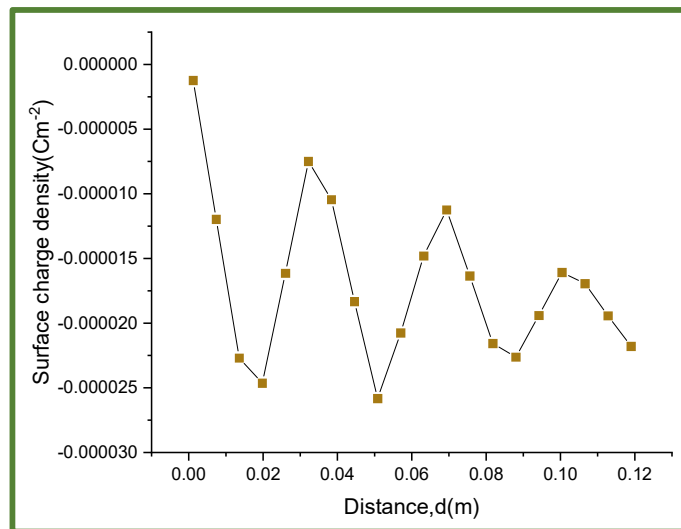


Fig 4.10 Surface charge density (Cm⁻²) versus separation distance, d(m) for short the circuit mode, i.e., when the electrodes are grounded and the floating potential is removed.

The variation in surface charge density of TENG as calculated by equation (2) is shown in figure 4.10 and when the dielectric constant value is set to 1 unit (figure 12), a linear curve is observed. The non-uniform variation in the surface charge density is because of the dielectric constant which depends on the thin film of polyethylene. When the dielectric constant value is set to 1, then even in free-standing mode the surface charged density (figure 4.11) is linearly increased with respect to the distance of separation.

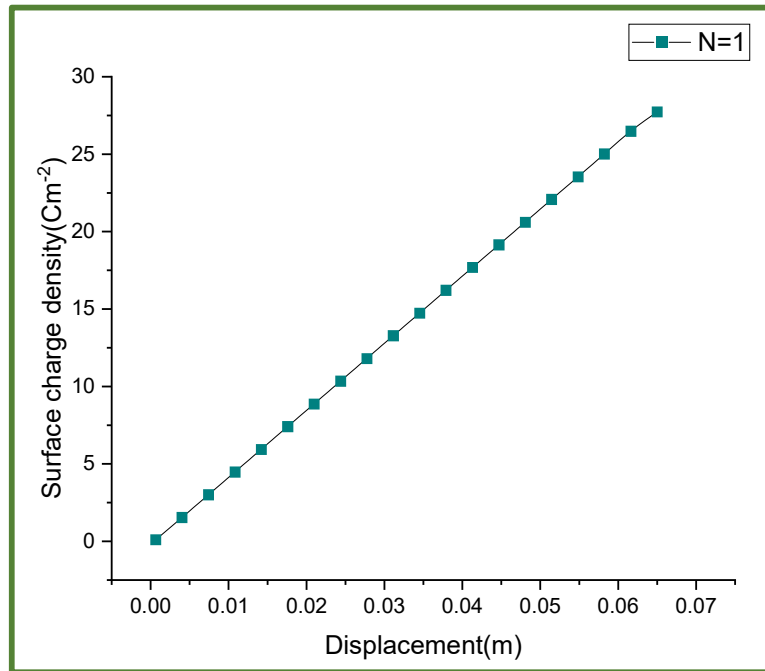


Fig 4.11 Surface charge density versus displacement(m) when dielectric constant=1

TENG AS WEARABLE DEVICES IN IoT

IoT is the internet of things that are embedded with sensors, power backups, software, and other technologies. TENGs have the capability of converting mechanical energy into electrical signals. The principle behind TENG being used in IoT is that whenever there is a motion, i.e., mechanical or kinetic energy, the contact separation in the respective modes of TENG changes and there is a high output voltage. This change in the open-circuit voltage can be utilized in two ways. First for sensing the motion and the rate of motion. For example, smartwatches can detect the intensity of motion by the change in the contact separation of the electrodes. Secondly, the mechanical energy that is converted into electrical signals can now be used to charge the watch and hence act as a power management system. The application of TENG in IoT and electronic Power management has been depicted in the following diagram.

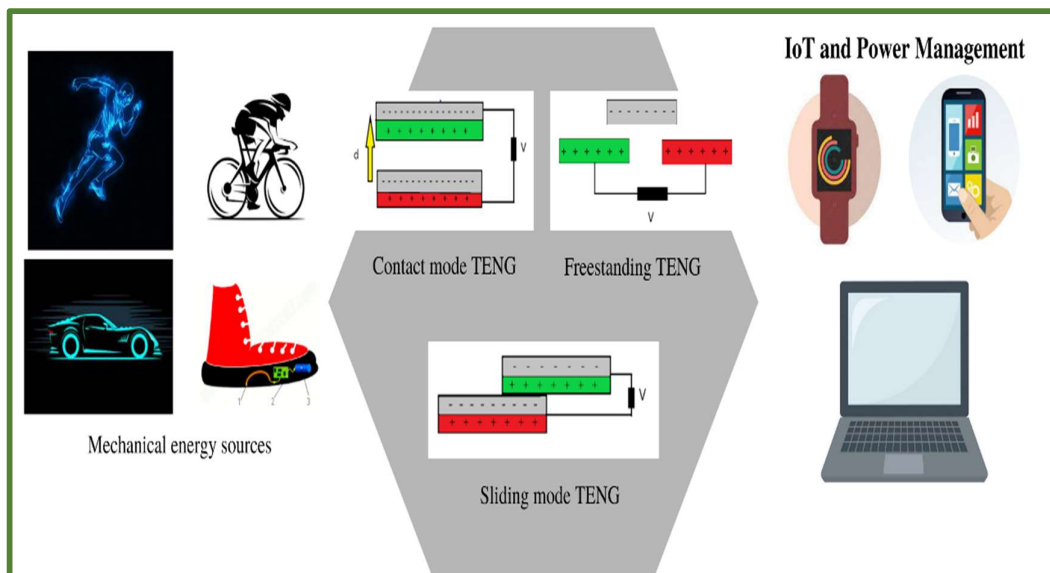


Fig 4.12 Application of TENG in IoT and electronic Power management

For TENG based sensors, the voltage sensitivity can be calculated by the equation,[20]

$$S_v = \frac{dV}{ds} \quad (4)$$

Where, dV is the change in voltage, ds is the change in the distance. So, the following are the sensitivities in Vm^{-1} for the respective sensors.

Table 4.1 Sensitivities of different modes of TENG based sensors

Type of TENG sensor	Sensitivity
Contact mode	64000 Vm ⁻¹
Sliding mode	0.77x 10 ⁻⁵ Vm ⁻¹
Freestanding mode	3,00,000 Vm ⁻¹

CHAPTER 5:
CONCLUSION
AND
FUTURE SCOPE

CONCLUSION

For the current developments and revolution in the fields of Internet of Things and Power Harvesting nowadays, the **Triboelectric Nanogenerator based sensors** are evolving many folds. The three-dimensional TENG has been designed and analysed for all the modes, namely contact mode, sliding mode, and the free-standing mode. The electric field norms-based simulation and results for each mode of the TENG model have been shown. For contact mode, when contact separation is varied, the open-source voltage increases up to a point, and then the increment is slow and the surface charge density has also shown similar variation. For sliding mode, there is a less increase in open-source voltage, however, the surface charge density has shown a steep increase. The best results have been shown by the freestanding mode in terms of sensitivity. The sensitivity is of the value of $3 \times 10^5 Vm^{-1}$. For open-source voltage and surface charge density, there is a zig-zag pattern. However, there is a linear variation of surface charge density of the free-standing mode when the dielectric constant value is equal to 1. The different modes of TENG are basically used for different applications and have great advantages in the field of IoT and power harvesting-based devices.

FUTURE SCOPE

Based on the developments and advancements in the fields of Internet of Things (IoT) and power harvesting, the Triboelectric Nanogenerator (TENG) based sensors have shown significant progress. In this paper, a three-dimensional TENG has been designed and analysed for various modes including contact mode, sliding mode, and free-standing mode. The simulations and results based on electric field norms have been presented for each mode of the TENG model. The results obtained from the contact mode analysis demonstrate that as the contact separation varies, the open-source voltage initially increases up to a certain point, after which the increment becomes slower. The surface charge density exhibits a similar variation pattern. In the sliding mode, there is a comparatively lower increase in the open-source voltage, but the surface charge density shows a steep increase. On the other hand, the free-standing mode exhibits the best results in terms of sensitivity, with a sensitivity value of $3 \times 10^5 \text{ Vm}^{-1}$. The open-source voltage and surface charge density in this mode demonstrate a zig-zag pattern. Interestingly, when the dielectric constant value is equal to 1, there is a linear variation in the surface charge density of the free-standing mode. These different modes of the TENG have diverse applications and offer significant advantages in the field of IoT and power harvesting-based devices. The findings of this research highlight the potential of TENG-based sensors for various applications in the future [26].

Based on these results, the future scope of this study can be outlined as follows:

1. **Optimization of TENG Design:** Further research can focus on optimizing the design of the TENG for enhanced performance. This can involve exploring different materials, configurations, and geometries to maximize power generation and sensitivity. Additionally, investigations can be conducted to determine the optimal contact separation distance and other parameters to achieve improved performance.
2. **Integration with IoT Systems:** The integration of TENG-based sensors with IoT systems presents numerous opportunities. Future work can explore the development of smart and self-powered IoT devices by incorporating TENG sensors into various applications such as environmental monitoring, healthcare, structural health monitoring, and wearable technologies. This integration can enable energy-efficient and sustainable IoT solutions.
3. **Enhancement of Sensitivity:** Efforts can be made to further enhance the sensitivity of TENG-based sensors. This can involve exploring novel materials, surface modifications, and electrode

configurations to achieve higher sensitivity and detection limits. The aim would be to improve the ability of TENG sensors to detect and measure subtle changes in the environment or physical parameters.

4. **Real-world Implementation:** Future research can focus on translating the laboratory-based findings into real-world applications. This may involve addressing challenges related to scalability, reliability, and durability of TENG-based sensors. Prototyping and testing in relevant environments can provide valuable insights into the feasibility and practicality of deploying TENG sensors in various industries and domains.
5. **Energy Harvesting Applications:** The power harvesting capabilities of TENG can be further explored and harnessed for practical applications. Future studies can investigate the integration of TENG with energy storage devices and power management systems to develop self-powered devices or systems. This can contribute to the development of energy-autonomous systems that rely on harvested energy from the surrounding environment.
6. **Multi-modal TENG Systems:** The combination of multiple TENG modes or the development of multi-modal TENG systems can be an interesting avenue for future exploration. Investigating the synergistic effects and capabilities of different TENG modes working together can lead to the development of more versatile and efficient energy harvesting and sensing systems. [27,28]

REFERENCES

- [1] Wang, Yannan Xie, Simiao Niu, Long Lin, and Zhong Lin Wang, Freestanding Triboelectric-Layer-Based Nanogenerators for Harvesting Energy from a Moving Object or Human Motion in Contact and Non-contact Modes, *Adv. Mater.* 2014, 26, 2818–2824.
- [2] Tao Li, || Jingdian Zou, || Fei Xing, Meng Zhang, Xia Cao, Ning Wang, and Zhong Lin Wang, From Dual-Mode Triboelectric Nanogenerator to Smart Tactile Sensor: A Multiplexing Design, *American Chemical Society Nano*.
- [3] Amjadi, M.; Kyung, K. U.; Park, I.; Sitti, M. Stretchable, SkinMountable, and Wearable Strain Sensors and Their Potential Applications: A Review. *Adv. Funct. Sihong Mater.* 2016, 26, 1678–1698.
- [4] Fang, Y.; Yashin, V. V.; Levitan, S. P.; Balazs, A. C. Pattern Recognition with Materials that Compute. *Sci. Adv.* 2016, 2, e1601114.
- [5] Wang, X.; Dong, L.; Zhang, H.; Yu, R.; Pan, C.; Wang, Z. L. Recent Progress in Electronic Skin. *Adv. Sci.* 2015, 2, 1500169.
- [6] Gong, S.; Schwalb, W.; Wang, Y.; Chen, Y.; Tang, Y.; Si, J.; Shirinzadeh, B.; Cheng, W. A Wearable and Highly Sensitive Pressure Sensor with Ultrathin Gold Nanowires. *Nat. Commun.* 2014, 5, 3132.
- [7] Wang, H.; Pastorin, G.; Lee, C. Toward Self-Powered Wearable Adhesive Skin Patch with Bendable Microneedle Array for Transdermal Drug Delivery. *Adv. Sci.* 2016, 3, 1500441.
- [8] Wang, C.; Hwang, D.; Yu, Z.; Takei, K.; Park, J.; Chen, T.; Ma, B.; Javey, A. User-Interactive Electronic Skin for Instantaneous Pressure Visualization. *Nat. Mater.* 2013, 12, 899–904.
- [9] Lee, H.-K.; Chang, S.-I.; Yoon, E. A Flexible Polymer Tactile Sensor: Fabrication and Modular Expandability for Large Area Deployment. *J. Microelectromech. Syst.* 2006, 15, 1681–1686.
- [10] Guang Qin Gu, Chang Bao Han, Cun Xin Lu, Chuan He, Tao Jiang, Zhen Liang Gao, Cong Ju Li, and Zhong Lin Wang, Triboelectric Nanogenerator Enhanced Nanofiber Air Filters for Efficient Particulate Matter Removal, *ACS Paragon Plus Environment, ACS Nano*.
- [11] Mildred S. Dresselhaus, Gang Chen, Ming Y. Tang, Ronggui Yang, *New Directions for Low-Dimensional Thermoelectric Materials, Adv. Mater.* 2007, 19, 1043–1053.
- [12] Zhong Lin Wang, *Triboelectric Nanogenerators as New Energy Technology for Self-Powered Systems and as Active Mechanical and Chemical Sensors, ACS Nano*.
- [13] Henniker, J. Triboelectricity in Polymers. *Nature* 1962, 196, 474
- [14] Fan, F. R.; Lin, L.; Zhu, G.; Wu, W. Z.; Zhang, R.; Wang, Z. L. Transparent Triboelectric Nanogenerators and Self-Powered Pressure Sensors Based on Micropatterned Plastic Films. *Nano Lett.* 2012, 12, 3109–3114.

- [15] Zhu, G.; Pan, C. F.; Guo, W. X.; Chen, C. Y.; Zhou, Y. S.; Yu, R. M.; Wang, Z. L. Triboelectric-Generator-Driven Pulse Electrodeposition for Micropatterning. *Nano Lett.* 2012, 12, 4960–4965.
- [16] Sihong Wang,[†] Simiao Niu, [†] Jin Yang,[†] Long Lin,[†] and Zhong Lin Wang, Quantitative Measurements of Vibration Amplitude Using a Contact-Mode Freestanding Triboelectric Nanogenerator, *ACS Nano*, 10.1021/nn5054365.
- [17] Weiqing Yang , Jun Chen , Qingshen Jing , Jin Yang , Xiaonan Wen, 3D Stack Integrated Triboelectric Nanogenerator for Harvesting Vibration Energy, *Adv. Funct. Mater.* 2014, 24, 4090–4096.
- [18] Yang, W. Q.; Chen, J.; Jing, Q. S.; Yang, J.; Wen, X. N.; Su, Y. J.; Zhu, G.; Bai, P.; Wang, Z. L., 3D Stack Integrated Triboelectric Nanogenerator for Harvesting Vibration Energy. *Adv. Funct. Mater.* 2014, 24, 4090-4096.
- [19] Zhang, C.; Tang, W.; Han, C. B.; Fan, F. R.; Wang, Z. L., Theoretical Comparison, Equivalent Transformation, and Conjunction Operations of Electromagnetic Induction Generator and Triboelectric Nanogenerator for Harvesting Mechanical Energy. *Adv. Mater.* 2014, 26, 3580-3591.
- [20] Han, C. B.; Jiang, T.; Zhang, C.; Li, X. H.; Zhang, C. Y.; Cao, X.; Wang, Z. L., Removal of Particulate Matter Emissions from a Vehicle Using a Self-Powered Triboelectric Filter. *ACS Nano*. 2015, 9, 12552– 12561.
- [21] Han, C. B.; Zhang, C.; Tang, W.; LI, X. H.; Wang, Z. L., High Power Triboelectric Nanogenerator based on Printed Circuit Board (PCB) Technology. *Nano Res.* 2015, 8, 722-730.
- [22] Kocik, M.; Dekowski, J.; Mizeraczyk, J., Particle Precipitation Efficiency in an Electrostatic Precipitator. *J. Electrostat.* 2005, 63, 761-766.
- [23] A. Al-Fuqaha, M. Guizani, M. Mohammadi, M. Aledhari, M. Ayyash, Internet of things: A survey on enabling technologies, protocols, and applications, *IEEE Commun. Surv. Tutorials.* 17 (2015) 2347–2376.
- [24] Z.L. Wang, J. Song, Piezoelectric nanogenerators based on zinc oxide nanowire arrays, *Science* 312 (2006) 242–246.
- [25] Z.L. Wang, J. Chen, L. Lin, Progress in triboelectric nanogenerators as a new energy technology and self-powered sensors, *Energy Environ. Sci.* 8 (2015) 2250–2282.
- [26] Z.L. Wang, Triboelectric nanogenerators as new energy technology for selfpowered systems and as active mechanical and chemical sensors, *ACS Nano* 7 (2013) 9533–9557.
- [27] R. Zhang, M. Hummelgård, J. Ortegren, M. Olsen, H. Andersson, H. Olin, Interaction of the human body with triboelectric nanogenerators, *Nano Energy* 57 (2019) 279–292.
- [28] J.H. Zhang, Y. Zhang, N. Sun, Y. Li, J. Du, L. Zhu, X. Hao, Enhancing output performance of triboelectric nanogenerator via large polarization difference effect, *Nano Energy* 84 (2021), 105892.

PLAGIARISM REPORT



Similarity Report ID: oid:27535:36296291

7% Overall Similarity

Top sources found in the following databases:

- 4% Internet database
- Crossref database
- 5% Submitted Works database
- 4% Publications database
- Crossref Posted Content database

Vishwas Kumar
VISHWAS
KUMAR

TOP SOURCES

The sources with the highest number of matches within the submission. Overlapping sources will not be displayed.

1	Loughborough University on 2020-09-02	<1%
	Submitted works	
2	Cheng, Gang, Zong-Hong Lin, Zu-liang Du, and Zhong Lin Wang. "Simult...	<1%
	Crossref	
3	University of Wales, Bangor on 2012-11-05	<1%
	Submitted works	
4	nanoscience.gatech.edu	<1%
	Internet	
5	matin.gatech.edu	<1%
	Internet	
6	mdpi.com	<1%
	Internet	
7	Manchester Metropolitan University on 2023-05-26	<1%
	Submitted works	
8	Zhong Lin Wang, Long Lin, Jun Chen, Simiao Niu, Yunlong Zi. "Triboele...	<1%
	Internet	

PUBLISHED PAPER

2022 4th International Conference on Advances in Computing, Communication Control and Networking (ICAC3N)

Designing and Analysis of Different Modes of Triboelectric Nanogenerator-based Sensors for IOT

Vishwas Kumar

Department of Applied
Physics, Delhi
Technological
University, Delhi, 110042,
Indiavishwaskr786@gmail.
com

Deepak Kumar

Department of Applied
Physics, Delhi
Technological University,
Delhi, 110042,
Indiakarndeepak11@gmail.
com

Mukta Sharma

Department of Applied
Physics, Delhi
Technological
University, Delhi, 110042,
Indiamuktasharma2912@g
mail.com

Prof. Vinod

Singh Department of
Applied Physics, Delhi
Technological
University, Delhi, 110042,
Indiavinodsingh@dtu.ac.in

Abstract— Today, the world has shifted towards IoT and Power conversion methods. For this, there are various traditional methods, but the need for energy in those methods is huge. Triboelectric generators are nanostructures with fast recovery, robust mechanisms, compact structures, and highly efficient systems. Triboelectric generators are self-powered and can sense changes due to mechanical energy and convert them into electrical energy as well. TENGs are basically divided into three categories, contact mode, sliding mode, and freestanding mode. The objective of this paper is to design and analyze the structure and parameters of these three modes of TENGs and to demonstrate their applications in the field of IoT, sensors, Power conservation as well as Power generation. The designed structure can detect the changes in the separation between the electrodes as small as of the order of a few millimeters. We have compared the properties and characteristics of these three modes with each other and have plotted the curves for the variation of open-circuit voltage and the surface charge densities for a short circuit with the change in the separation of electrodes. Along with the ability of this generator to analyze the changes in the separation due to external parameters, it can also give information about the extent to which it gets impacted. The voltage sensitivities of the sensor are as high as $64,000\text{Vm}^{-1}$ for contact mode and $3,00,000\text{Vm}^{-1}$ for the freestanding mode of the TENG sensor.

Keywords - *Triboelectric Nanogenerator, Nanosensors, Nanoelectronics, Electrical transport, Energy conservation*

INTRODUCTION

In recent years, with the large-scale development of nanotechnology, the use of nanotechnology and nanostructures in solving modern-day problems has been immense. From homes to industries, smart devices are a need in our day-to-day life. There are various kinds of existing devices like capacitive pressure sensors, electromechanical sensors, optical sensors, resistive sensors, and various air filters like carbonated ones, charcoal-based and electrochemical ones[1-5]. However, the functioning of such devices depends on energy due to which there are many issues like frequent battery changes, use of non-renewable energy resources, difficulties to operate in remote areas, etc.[6,7] Thus, there occurs a need to develop such devices that are based on smaller structures that are not difficult to carry

and are highly efficient. To overcome these limitations, the use of triboelectric nanogenerators has increased many folds. Triboelectric nanogenerators (TENG) are basically conversion units from mechanical to electrical energy [8]. TENGs are basically based on two different principle phenomena, namely Contact electrification and Electrical Induction. Contact electrification happens when two or more objects arrive within close proximity to each other. With the proximity of the surfaces, the electric charges get induced on the surfaces. Whereas electrical Induction is the phenomenon of an electrical conductor becoming electrically charged whenever it comes in contact with a charged body [9,10]. Due to these major phenomena, the TENGs have fast response, compact and flexible structures, high efficiency, and low detection limits. The triboelectric generator has three operating modes, namely, the contact mode, the sliding mode, and the free-standing mode [11]. In the contact mode, the triboelectric layers are connected with a mechanical source and the other one with a lead wire. In the sliding mode, the top layer of the generator is horizontally movable and the distance can be varied between the ends of the top and the bottom layer horizontally. The free-standing mode basically has three layers with two of the layers being below the top layer separated by a distance and the two layers below the top layer lie on the same level with a constant separation [12]. The wearable devices based on triboelectric generators are based on the contact and the sliding modes. However, if there is a need for the device to be versatile and its functionality to be associated with any arbitrary object, it is important to use the Freestanding mode of the Triboelectric generator.[13-14] The triboelectric generator consists of multiple layers each connected with electrodes there is a continuous alternating current flowing between them and when there are external mechanical factors involved, there is an induction of opposite static charges on the different layers of the generator[15]. The output of a Triboelectric nanogenerator is such that the Voltage is high with low current and high intrinsic impedance. The first Freestanding based Triboelectric nanogenerator was demonstrated by Sihong Wang in 2014[16].Owing to the existing literature, the Triboelectric nanogenerators are

2022 4th International Conference on Advances in Computing, Communication Control and Networking (ICAC3N) | 978-1-6654-7436-8/22/\$31.00 ©2022 IEEE | DOI: 10.1109/ICAC3N56670.2022.10074560

ISBN: 978-1-6654-7436-8/22/\$31.00 ©2022 IEEE

1425

Authorized licensed use limited to: Indraprastha Institute of Information Technology. Downloaded on May 22, 2023 at 10:11:31 UTC from IEEE Xplore. Restrictions apply.

widely being demonstrated and used as energy harvesting systems based on sustainable resources[17,18]. From sensing technologies[19] to IOT[20,21] and for air filtration[22], triboelectric nanogenerators are widely being used. The traditional triboelectric generators were basically the ones that were used to create static electricity from contact charges. A well-known example of a Triboelectric generator is the Van-De-Graaf generator and the Wimshurst machine. These two generators were invented in 1929 and 1880 respectively. These generators are used to accumulate large charge values through corona discharge and used to produce a high voltage output with no current without discharging. However, the structures of these generators are known and cannot be used for a device as compact as a smartwatch or a heart rate monitoring sensor. This caused the need for the development of Triboelectric nanogenerators. TENGs can be operated in a self-powered mode are provided with a constant capacitance and a fixed electric field.

In this paper, the three modes of Triboelectric nanogenerator are designed, analyzed and their efficiencies are calculated as well as compared. The TENG has positive electrodes of metal oxide Al_2O_3 . Al_2O_3 has been taken because of its stability and conductivity of charge, while polyethylene has been taken as the negative electrode and it is acting as the dielectric. The variation of open source and short circuit voltages has been shown with respect to the contact separation between the layers of the nanogenerator. The range of the contact separation between the layers of the generator is in a few millimeters while voltages are in Volts. Also, the surface charge density for the short circuit of the nanogenerator has been calculated and varied with respect to the separation. The applications of the TENG have been shown in smart devices. The smart sensor based on a contact-based TENG has been demonstrated and the efficiency is also calculated. The applications of the TENG-based sensors are shown in common use and for energy harvesting. The TENG is a self-powered device because the mechanical energy changes into electrical energy so, this generator can be used in various devices to sense the changes in electric current due to motion with a calculated maximum sensitivity of the order of 10^5 Vm^{-1} .

I. STRUCTURAL DESIGN AND ANALYSIS

The proposed structure of the TENG basically needs a design such that on applying an external source of electricity, there is an induction of the charges and the separated charges develop more and lead to the self-generated electric field so that with more variation in the separation, more deflection in the open-source and even short circuit voltages is obtained. Therefore, the vertical separation-based TENGs are designed with two layers being stacked with a separation of the order of millimeters. The contact separation mode of the TENG is shown in fig.1a. This mode of the generator basically has

two layers with a vertical separation of d millimeters. On applying the external voltage, V , there is an induction of charges with opposite charges being induced on the surfaces that are close to each other while on the surfaces that are opposite have the same charges as each other. Although, the vertical separation of charges shows high efficiency in calculating the frequency of the generator but is not that efficient for amplitude calculation. Thus, there are two other developed modes of TENG. The sliding mode TENG as shown in figure 1b, has a horizontal separation between the ends of the two electrodes stacked in contact with each other. The voltage is applied and the horizontal distance is varied in this mode and with the variation of the horizontal distance known as the sliding distance, the open circuit, and the short circuit voltage variations are noted down. The recently developed and the most efficient mode of TENG is the free-standing mode (shown in figure 1c). The free-standing mode has two electrodes resting in the same plane with a movable electrode lying in a plane above them at a constant vertical separation and slides between both the layers beneath it. The free-standing mode of TENG has a more efficient energy harvesting structure free from electrodes, has higher stability, and can be used for any arbitrary moving objects. Due to its unique and stable structure, free-standing TENG is most widely used for its applications in the Internet of Things and power harvesting.

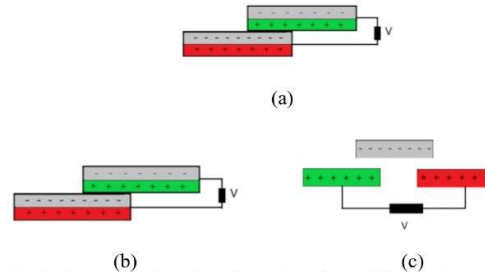


Fig.1. Structure and working illustration of the Triboelectric generator with the stacking of positive and negative layers. (a) Circuit diagram showing TENG in contact separation mode with a contact separation of d millimeters. (b) Circuit diagram of TENG in contact sliding mode with the positive and negative charges separated and connected with voltage source V . (c) Circuit diagram of TENG in free-standing mode with the positive and negative charges separated and connected with voltage source V .

In our model, the electrodes are built with Alumina or aluminium oxide due to its stable and highly conducting nature. The upper layer is basically Polyethylene film of the thickness of the order of $50\mu\text{m}$. The material Polyethylene is chosen because it has negative polarity for triboelectric generator and there these two materials are stacked together in terms of acrylic sheets. The Al_2O_3 electrodes are put at positive while the Polyethylene is put at negative for electrolyzing the TENG due to their respective natures towards the triboelectric phenomenon. Now, the separation d is first of all set at about 0.001m

between the respective electrodes which is then varied up to 0.020 for the contact mode. For the sliding mode, the horizontal sliding distance is initially set at 1mm and then is varied up to 100 mm. For the freestanding mode, initially, the separation is set to 0.01m and is varied up to 0.05m. For each separation value of all the modes of TENG, the corresponding open source voltages and the short circuit surface charge density are noted down. Therefore, for the contact mode TENG, the distance d between the electrodes is varied. For the sliding mode TENG, the distance d between the electrodes is fixed and the sliding distance towards the x-axis is varied while for free-standing mode, the distance d is varied in order to observe the corresponding changes in the open-source voltage and the surface charge densities[7]. After defining the parameters for the contact, sliding and the free standing modes, the geometry is built by taking the rectangles and setting their positions such that the structure for each mode is built. The geometry of the TENGs the following structures(Fig.2.) are obtained in the software. The parameters that have been chosen for this model are Length (Al_2O_3 electrodes)=0.064m, Thickness(Al_2O_3 electrodes)= 10^{-5} m, Length(Polyethylene dielectric)=0.064m, Thickness(Polyethylene dielectric)= 10^{-4} m, Separation(d)=0.01-0.065m.

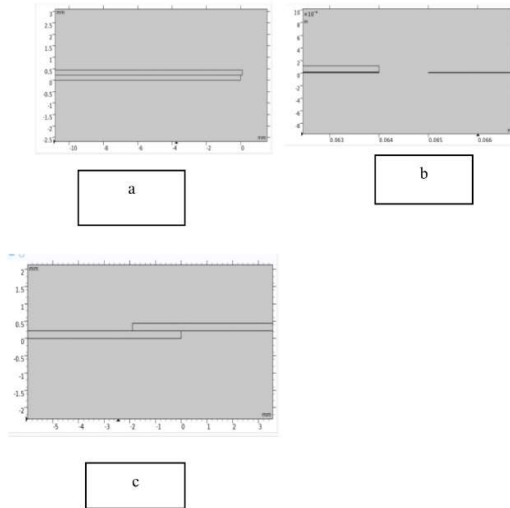


Fig.2. The designed geometry for the TENG modes with stacked layers with the top and bottom layers being Al_2O_3 electrodes and in the middle being the thin nanofilm of polyethylene. (a) Layers of electrodes for contact mode with contact separation being of the order of a few millimeters (b) The designed structure for the sliding layers of the sliding mode TENG. (c) Freestanding mode designed structure for TENG with two electrodes below and single electrode above them and the polyethylene film between the electrodes.

The reason behind creating the layer of Polyethylene is that Polyethylene is an electret material and due to the presence of the thin film of Polyethylene, the induced charges are preserved on the surface for a long time and then the resulting open-source voltage and the surface charge densities in the short circuit are observed for a long time even when there is no voltage applied from the external sources. The presence of Polyethylene is the main source of self-operating power for the TENG contact, sliding, and free-standing modes. The meshed structure of each mode is shown in figure 3 to configure the details of the structure and the applied electric field.

II. RESULTS AND SIMULATIONS

A. Contact mode TENG

After designing the geometry of the contact mode, the materials are selected and the voltage is applied at the electrodes with a constant contact separation of 0.01m. After application of the voltage to the electrodes, there is free potential applied to each surface and thus, there is a generation of the electric field between the electrodes and in the external surrounding medium which is taken as air. The electric field norm is run for the stationary frequency mode analysis of the contact mode TENG model, then, the obtained model showing the distribution of electric field is as shown in figure 4. The figure basically shows the surface electric potential lying between the electrodes when the separation is changed from 0.06 to 0.013 meters. The electric field cloud is increasing with an increase in contact separation which is basically shown by the blue and red colored fields taken. The positive and the negative charges are thus induced and when there is a short circuit applied the induced charges generate a surface charge density which also depends on the contact separation as is further shown in the curves.

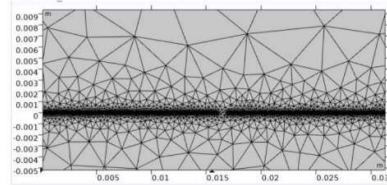


Fig.3. The mesh structure for the TENG geometry showing the minute details of the electrodes and their separation.

The variation in the contact mode separation, d yields an increment in open circuit potential difference(V) , which

is high from distance 0 to 0.015m and then a slow increment is there with distance. This variation is seen in figure 4. The open-circuit voltage can be calculated by the following equation[6],

$$V = \frac{\sigma d}{\epsilon_0} \quad (1)$$

Where, σ is the triboelectric charge density which is predefined and ϵ_0 is the permittivity of free space.

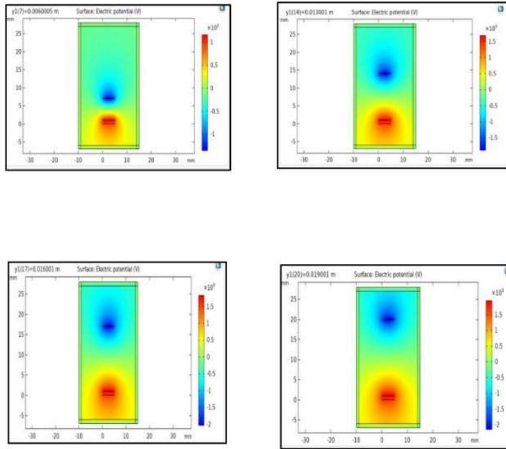
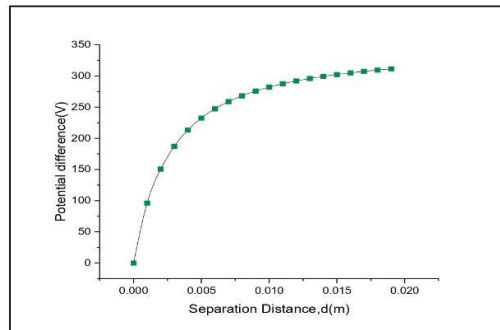


Fig.4. Electric field norm of contact mode TENG showing the distribution of the electric field when the electrodes that are positive and negative are close to each other. With the Polyethylene layer being negative and the Al_2O_3 layers being positive. The distance of separation for (a)d=0.006m (b)d=0.013m (c) d=0.016m and (d) d=0.019m.

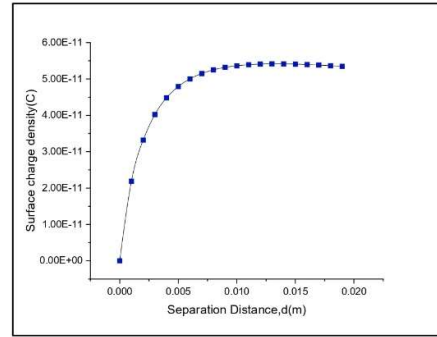
From fig.5, it is observed that after applying the free potentials to the surfaces of the electrodes there is a generation of the open-source voltage at a constant contact separation. When the contact separation is further increased, there is a linear increase observed in the value of open source voltage up to 0.005m. However, when the distance is further increased up to 0.020m, the rise in the open-source voltage is less and more of a constant or slightly rising curve is achieved.

The surface charge density is calculated by using the equation[7],



$$\sigma_m = \frac{BP\epsilon_0(d + \epsilon_r x)}{(\ln(Px) + C)d} \quad (2)$$

Fig. 5. Open circuit voltage versus contact separation distance curve showing the potential difference at the y-axis and the separation distance between the electrodes in meters at the x-axis.



where B and C are constants defined by the composition of material and pressure, P is atmospheric pressure of 101Pa, ϵ_0 , and ϵ_r are the permittivity of free space ($8.85 \times 10^{-12} Fm^{-1}$) and relative permittivity of the material medium, respectively. From figure 6, Therefore, the surface charged density is almost constant when the separation of the Al_2O_3 electrodes and the polyethylene thin film is from 0.010 to 0.020 meters. Whereas when the separation is of the order of a few millimeters there is a steep increase observed in the surface charge density.

Fig.6. Surface charge density (Cm^{-2}) versus separation distance, d(m) for short the circuit mode, i.e., when the electrodes are grounded and the floating potential is removed.

B. Sliding Mode

After fabricating the sliding mode geometrically, the materials are selected and the voltage is applied at the electrodes with a constant contact separation of 20.1mm. After application of the voltage to the electrodes, there is free potential applied to each surface and thus, there is a generation of the electric field between the electrodes and in the external surrounding medium which is taken as air. The electric field norm is run for the stationary frequency mode analysis of the sliding mode TENG model, then, the obtained model showing the distribution of electric field is as shown in figure 7. The figure basically shows the surface electric potential lying between the electrodes when the separation is changed from 20.1 to 98.1 millimeters. The electric field cloud is increasing horizontally with an increase in sliding separation which is basically shown by the blue, orange, and yellow-colored fields taken. The positive and the negative charges are thus induced and when there is a

short circuit applied the induced charges generate a surface charge density which also depends on the contact separation as is further shown in the curves.

The variation in the sliding mode separation, d yields a constant increment in open circuit potential difference (V), calculated by equation (1) which can be seen in figure 8. From figure 8, it is observed that after applying the free potentials to the surfaces of the electrodes there is a generation of the open-source voltage at a constant contact separation. When the contact separation is further increased, there is a total linear increase observed in the value of open source voltage up to 100mm. The open-source voltage of the sliding mode of the TENG is directly proportional to the sliding distance.

The variation in surface charge density of TENG as calculated by equation (2) is shown in figure 9.

Therefore, the surface charge density is almost constant when the separation of the Al_2O_3 electrodes and the polyethylene thin film is from 0 to 60 millimeters. Whereas when the separation is of the order of 60 to 100 millimeters there is a steep increase observed in the surface charge density.

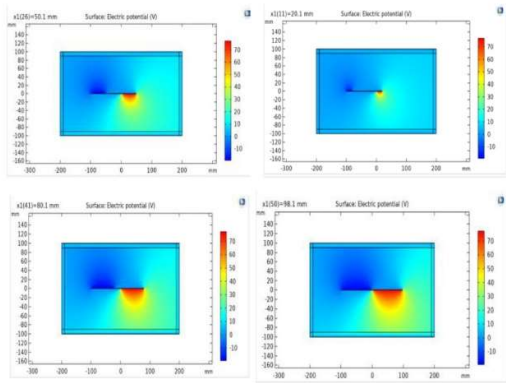


Fig.7. Electric field norm of the sliding mode TENG with showing the concentration of electric field near both the electrodes that are separated horizontally and the for the polyethylene film when the sliding distance (a)d=0.02m (b)d=0.05m (c) d=0.08m and (d) d=0.098m.

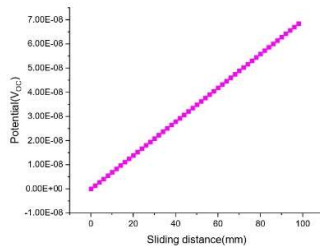


Fig. 8. Open circuit voltage versus sliding distance(mm) linear curve showing the open circuit potential difference at the y-axis and the separation distance between the electrodes in millimeters at x-axis.

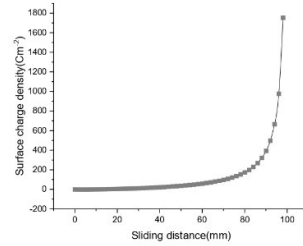


Fig.9. Surface charge density (Cm^{-2}) versus separation distance, d (mm) for short the circuit mode, i.e., when the electrodes are grounded and the floating potential is removed

C. Freestanding Mode

The designing of the free-standing mode after the materials are selected and the voltage is applied at the electrodes with a constant contact separation of 0.042975mm. After application of the voltage to the electrodes, there is free potential applied to each surface and thus, there is a generation of the electric field between the electrodes and in the external surrounding medium which is taken as air. The electric field norm is run for the stationary frequency mode analysis of the free-standing mode TENG model, then, the obtained model showing the distribution of electric field is as shown in figure 10. The figure basically shows the surface electric potential lying between the electrodes when the separation is changed from 0.04 to 0.11 meters. The electric field cloud is increasing horizontally with an increase in sliding separation which is basically shown by the blue, orange, green, and yellow-colored fields taken. The positive and the negative charges are thus induced and when there is a short circuit applied

the induced charges generate a surface charge density which also depends on the contact separation as is further shown in the curves.

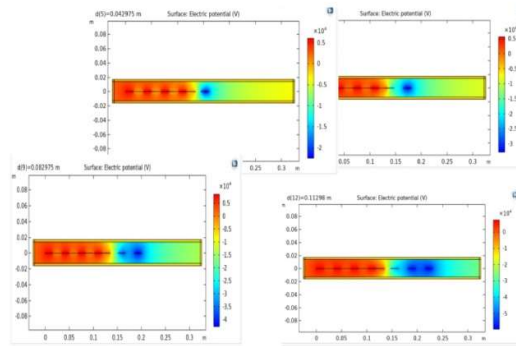


Fig.10.

Electric field norm of the sliding mode TENG with showing the concentration of electric field near both the electrodes that are separated horizontally and the for the polyethylene film when the free-standing vertical contact separation, (a)d=0.043m (b)d=0.062m (c) d=0.083m and (d) d=0.11m.

The variation in the freestanding mode separation, d yields a zig-zag pattern in variation of open circuit potential difference(V), calculated by equation (1), which can be seen in figure 11. The increase in the open-circuit voltage is observed when the distance is varied from 0 to 0.02 meters while there is a decrease in the open-circuit voltage from 0.02 to 0.03 meters and then, again, an increase in the open-source voltage is observed from 0.035 to 0.04 meters of contact separation followed by a decrease at the last 0.045-0.05 meters. The variation in surface charge density of TENG as calculated by equation (2) is shown in fig.12 and when the dielectric constant value is set to 1 unit(fig.12), a linear curve is observed. The non-uniform variation in the surface charge density is because of the dielectric constant which depends on the thin film of polyethylene. When the dielectric constant value is set to 1, then even in free-standing mode the surface charged density(fig.13) is linearly increased with respect to the distance of separation.

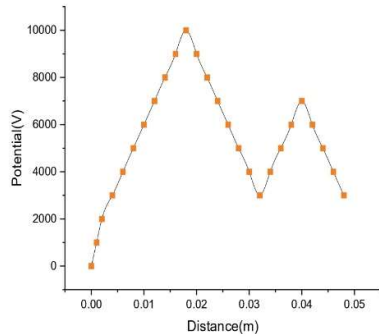


Fig.11. Open circuit voltage versus sliding distance(m) linear curve showing the open circuit potential difference at the y-axis and the separation distance between the electrodes in millimeters at the x-axis.

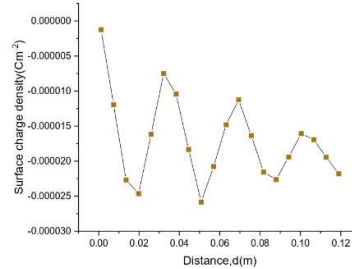


Fig.12. Surface charge density (Cm⁻²) versus separation distance, d(m) for short the circuit mode, i.e., when the electrodes are grounded and the floating potential is removed.

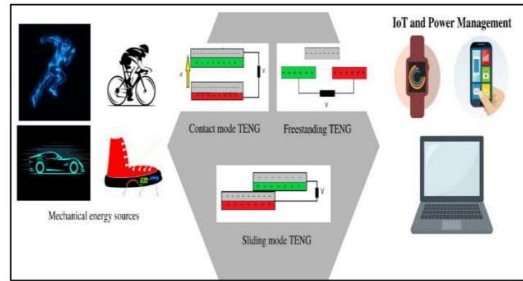


Fig.13. Surface charge density versus displacement(m) when dielectric constant=1

III. TENG AS WEARABLE DEVICES IN IoT

IoT is the internet of things that are embedded with sensors, power backups, software, and other technologies. TENGs have the capability of converting mechanical energy into electrical signals. The principle behind TENG being used in IoT is that whenever there is a motion, i.e., mechanical or kinetic energy, the contact separation in the respective modes of TENG changes and there is a high output voltage. This change in the open-circuit voltage can be utilized in two ways. First for sensing the motion and the rate of motion. For example, smart watches can detect the intensity of motion by the change in the contact separation of the electrodes. Secondly, the mechanical energy that is converted into electrical signals can now be used to charge the watch and hence act as a power management system. The application of TENG in IoT and electronic Power management has been depicted in the following diagram.

For TENG based sensors, the voltage sensitivity can be calculated by the equation,[20]

$$S_v = \frac{dV}{ds} \quad (4)$$

Where, dV is the change in voltage, ds is the change in the distance. So, the following are the sensitivities in Vm^{-1} for the respective sensors.

Table.1. Sensitivities of different modes of TENG based sensors

Type of TENG sensor	Sensitivity
Contact mode	64000 Vm^{-1}
Sliding mode	0.77x 10 ⁵ Vm^{-1}
Freestanding mode	3,00,000 Vm^{-1}

The different sensitivities for the different modes are the building reason for the different applications of each mode of TENG. In IoT and various sensors-based devices, the freestanding mode is the most commonly used. The reason for this is its stability and its reaction and efficiency towards any arbitrary object and also its efficient measurement of the amplitude as well as frequency. The contact mode also has a significant value of efficiency and

Fig.14. Diagram for TENG as IoT devices and power management systems

thus, can be used as a sensor (figure 14) as well as the Power conservation device. The sliding mode is basically used for Power conversation and other flexible devices as well.

IV. CONCLUSION

For the current developments and revolution in the fields of Internet of Things and Power Harvesting nowadays, the triboelectric nanogenerator is evolving many folds. The three-dimensional TENG has been designed and analysed for all the modes, namely contact mode, sliding mode, and the free-standing mode. The electric field norms-based simulation and results for each mode of the TENG model have been shown. For contact mode, when contact separation is varied, the open-source voltage increases up to a point, and then the increment is slow and the surface charge density has also shown similar variation. For sliding mode, there is a less increase in open source voltage, however, the surface charge density has shown a steep increase. The best results have been shown by the freestanding mode in terms of sensitivity. The sensitivity is of the value of $3 \times 10^5 Vm^{-1}$. For open-source voltage and surface charge density, there is a zig-zag pattern. However, there is a linear variation of surface charge density of the free-standing mode when the dielectric constant value is equal to 1. The different modes of TENG are basically used for different applications and have great advantages in the field of IoT and power harvesting-based devices.

ACKNOWLEDGMENT

We are thankful to Dr. Vinod Singh for guiding us through this project work

REFERENCES

- [1] Wang, Yannan Xie, Simiao Niu, Long Lin, and Zhong Lin Wang, Freestanding Triboelectric-Layer-Based Nanogenerators for Harvesting Energy from a Moving Object or Human Motion in Contact and Non-contact Modes, *Adv. Mater.* 2014, 26, 2818–2824.
- [2] Tao Li, Jingdian Zou, Fei Xing, Meng Zhang, Xia Cao, Ning Wang, and Zhong Lin Wang, From Dual-Mode Triboelectric Nanogenerator to Smart Tactile Sensor: A Multiplexing Design, *American Chemical Society Nano.*
- [3] Amjadi, M.; Kyung, K. U.; Park, I.; Sitti, M. Stretchable, Skin-Mountable, and Wearable Strain Sensors and Their Potential Applications: A Review. *Adv. Funct. Mater.* 2016, 26, 1678–1698.
- [4] Fang, Y.; Yashin, V. V.; Levitan, S. P.; Balazs, A. C. Pattern Recognition with Materials that Compute. *Sci. Adv.* 2016, 2, e1601114.
- [5] Wang, X.; Dong, L.; Zhang, H.; Yu, R.; Pan, C.; Wang, Z. L. Recent Progress in Electronic Skin. *Adv. Sci.* 2015, 2, 1500169.
- [6] Gong, S.; Schwalb, W.; Wang, Y.; Chen, Y.; Tang, Y.; Si, J.; Shirinzadeh, B.; Cheng, W. A Wearable and Highly Sensitive Pressure Sensor with Ultrathin Gold Nanowires. *Nat. Commun.* 2014, 5, 3132.
- [7] Wang, H.; Pastorin, G.; Lee, C. Toward Self-Powered Wearable Adhesive Skin Patch with Bendable Microneedle Array for Transdermal Drug Delivery. *Adv. Sci.* 2016, 3, 1500441.
- [8] Wang, C.; Hwang, D.; Yu, Z.; Takei, K.; Park, J.; Chen, T.; Ma, B.; Javey, A. User-Interactive Electronic Skin for Instantaneous Pressure Visualization. *Nat. Mater.* 2013, 12, 899–904.
- [9] Lee, H.-K.; Chang, S.-I.; Yoon, E. A Flexible Polymer Tactile Sensor: Fabrication and Modular Expandability for Large Area Deployment. *J. Microelectromech. Syst.* 2006, 15, 1681–1686.
- [10] Guang Qin Gu, Chang Bao Han, Cun Xin Lu, Chuan He, Tao Jiang, Zhen Liang Gao, Cong Ju Li, and Zhong Lin Wang, Triboelectric Nanogenerator Enhanced Nanofiber Air Filters for Efficient Particulate Matter Removal, *ACS Paragon Plus Environment, ACS Nano.*
- [11] Mildred S. Dresselhaus, Gang Chen, Ming Y. Tang, Ronggui Yang, New Directions for Low-Dimensional Thermoelectric Materials, *Adv. Mater.* 2007, 19, 1043–1053.
- [12] Zhong Lin Wang, Triboelectric Nanogenerators as New Energy Technology for Self-Powered Systems and as Active Mechanical and Chemical Sensors, *ACS Nano.*
- [13] Henniker, J. Triboelectricity in Polymers. *Nature* 1962, 196, 474
- [14] Fan, F. R.; Lin, L.; Zhu, G.; Wu, W. Z.; Zhang, R.; Wang, Z. L. Transparent Triboelectric Nanogenerators and Self-Powered Pressure Sensors Based on Micropatterned Plastic Films. *Nano Lett.* 2012, 12, 3109–3114.
- [15] Zhu, G.; Pan, C. F.; Guo, W. X.; Chen, C. Y.; Zhou, Y. S.; Yu, R. M.; Wang, Z. L. Triboelectric-Generator-Driven Pulse Electrodeposition for Micropatterning. *Nano Lett.* 2012, 12, 4960–4965.

- [16] Sihong Wang,† Simiao Niu,† Jin Yang,† Long Lin,† and Zhong Lin Wang, Quantitative Measurements of Vibration Amplitude Using a Contact-Mode Freestanding Triboelectric Nanogenerator, *ACS Nano*, 10.1021/nn5054365.
- [17] Weiqing Yang , Jun Chen , Qingshen Jing , Jin Yang , Xiaonan Wen. 3D Stack Integrated Triboelectric Nanogenerator for Harvesting Vibration Energy, *Adv. Funct. Mater.* 2014, 24, 4090–4096.
- [18] Yang, W. Q.; Chen, J.; Jing, Q. S.; Yang, J.; Wen, X. N.; Su, Y. J.; Zhu, G.; Bai, P.; Wang, Z. L., 3D Stack Integrated Triboelectric Nanogenerator for Harvesting Vibration Energy. *Adv. Funct. Mater.* 2014, 24, 4090–4096.
- [19] Zhang, C.; Tang, W.; Han, C. B.; Fan, F. R.; Wang, Z. L., Theoretical Comparison, Equivalent Transformation, and Conjunction Operations of Electromagnetic Induction Generator and Triboelectric Nanogenerator for Harvesting Mechanical Energy. *Adv. Mater.* 2014, 26, 3580–3591.
- [20] Han, C. B.; Jiang, T.; Zhang, C.; Li, X. H.; Zhang, C. Y.; Cao, X.; Wang, Z. L., Removal of Particulate Matter Emissions from a Vehicle Using a Self-Powered Triboelectric Filter. *ACS Nano*. 2015, 9, 12552– 12561.
- [21] Han, C. B.; Zhang, C.; Tang, W.; LI, X. H.; Wang, Z. L., High Power Triboelectric Nanogenerator based on Printed Circuit Board (PCB) Technology. *Nano Res.* 2015, 8, 722-730.
- [22] Kocik, M.; Dekowski, J.; Mizeraczyk, J., Particle Precipitation Efficiency in an Electrostatic Precipitator. *J. Electrostat.* 2005, 63, 761-766.